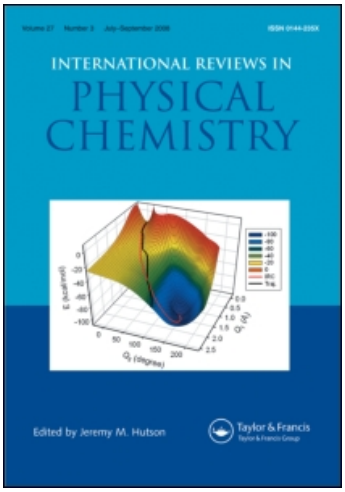

International Reviews in Physical Chemistry
Publication details, including instructions for authors and subscription information:
http://www.informaworld.com/smpp/title~content=t713724383

Energy bands in solids: bonding, energy levels and orbitals

Miklos Kertesz[a]
[a] Department of Chemistry, Georgetown University, Washington, DC, USA

To cite this Article Kertesz, Miklos(1985) 'Energy bands in solids: bonding, energy levels and orbitals', International Reviews in Physical Chemistry, 4: 2, 125 — 164
To link to this Article: DOI: 10.1080/01442358509353357
URL: http://dx.doi.org/10.1080/01442358509353357

INTERNATIONAL REVIEWS IN PHYSICAL CHEMISTRY, 1985, VOL. 4, NO. 2, 125–164

Energy bands in solids: bonding, energy levels and orbitals

by MIKLOS KERTESZ
Department of Chemistry, Georgetown University,
Washington, DC 20057, U.S.A.

Qualitative aspects of semiempirical energy band calculations are surveyed with the purpose of highlighting the key features of the electronic structures of some insulators, semiconductors and metallic systems. The nodal structure of the electronic orbitals is stressed as the common underlying theme in such effects as: the Peierls distortions of metallic systems; the changing electron counts (due to charge transfer or different *d*-electron counts); the high-pressure transformations of solids. The range of applicability of semiempirical non-self-consistent band theories is assessed. The discussion is illustrated by several examples.

1. Introduction

Along with the growth of solid-state sciences the language of solid-state physics as the theoretical framework of the field is penetrating solid-state chemistry. In this review we shall concentrate on one particular subject: semiempirical energy band theory, because it appears to have a major impact on our understanding of the properties and stabilities of complex crystalline compounds as well as seeming to have further potentialities in the global description of electrons in solids. We have made no effort to be comprehensive. Rather, we would like to point out in some depth the importance of the nodal structure of the one-electron orbitals—largely dictated by symmetry— using a rather arbitrarily picked set of examples from the recent literature. Several more comprehensive reviews on band structure calculations are readily available, see, for example, Callaway (1964), Bullett (1980) and Harrison (1980). This more elementary account, however, can be understood merely with some knowledge of molecular orbital theory. In fact, this area has been a place of cross fertilization of solid state and molecular ideas. Some concepts known in molecular quantum chemistry for a long time, have been rediscovered in the solid-state band field and vice versa. An example of the former may be the chemical pseudopotential (CP) of Anderson (1968, 1969) and Bullett (1975, 1980), which have their molecular counterparts in the Hückel (1931) and extended Hückel theories (EHT) (Hoffmann 1963). Examples of the latter are abundant: for instance, several research groups have discovered for themselves that periodic boundary conditions (p.b.c.) enable one to reduce the size of matrices from (in principle) infinity down to unit cell size once reciprocal lattice vectors are used. In fact, the first 'molecular orbital'—actually a crystal orbital—was written by Bloch (1928) for a solid, not a molecule in terms of the $\chi_\alpha(r)$ atomic orbitals, as a linear combination of atomic orbitals, LCAO

$$\psi_k(r) = 1/\sqrt{N} \sum_j \exp(ikR_j)\chi_\alpha(r - R_j) \tag{1}$$

Here the summation extends over the whole periodic lattice, defined by the lattice vectors

$$R_j = j_1 a_1 + j_2 a_2 + j_3 a_3 \tag{2}$$

The k wave-vectors (vectors in reciprocal or k space) are associated with every Bloch function through Bloch's theorem:

$$T_R\psi_k = \exp(ikR)\psi_k \tag{3}$$

where T_R is a translation operator corresponding to any lattice translation R. Bloch's theorem thus defines the k vector up to multiples of 2π in the phase of $\exp(ikR)$, in fact modulo reciprocal lattice vectors K_i, which are defined to make the scalar product $K_i a_l = 2\pi\delta_{il}$. Bloch theorem also gives us a conveneint way of determining k from the wavefunction. For example, for the following simple orbital of an infinite chain of H atoms (**1**) translation by one lattice vector changes the sign of the wavefunction, leading

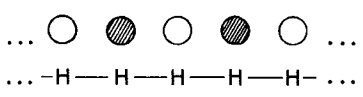

1

to $-1 = \exp(ikR)$, thus $k = \pi/a$. In other words the wave-vector, k, determines the relative phases of the orbitals in neighbouring unit cells.

Energy bands are the collections of permissible energy levels of a lattice, the eigenvalues of the corresponding Schrodinger equation:

$$H\psi_{nk}(r) = \varepsilon_n(k)\psi_{nk}(r) \tag{4}$$

where H is a one-electron Hamiltonian, such as Hartree–Fock, and n is the band index, allowing several solutions for a given k to occur. The $\varepsilon_n(k)$ values as a function of k are the energy bands.

In studying energy bands, substantial effort goes into establishing the *symmetry* properties (Heine 1960). Due to time-reversal symmetry:

$$\varepsilon_n(k) = \varepsilon_n(-k) \tag{5}$$

It can be shown that the reciprocal lattice (i_1, i_2, and i_3 integers)

$$K_i = i_1 K_1 + i_2 K_2 + i_3 K_3 \tag{6}$$

belongs to the same crystal system as the original direct lattice of R_j vectors. For example, if R_i forms a face centred cubic (f.c.c.) lattice, K_i forms a body-centred reciprocal lattice. Due to the periodicity of the K_i lattice, as well as the way it is constructed,

$$\exp(ikR_j) = \exp[i(k+K_i)R_j] \tag{6a}$$

for any R_j and K_i. Thus k vectors differing by multiples of reciprocal lattice vectors are called equivalent. It is convenient and customary to restrict the study of the energy bands to a small region, called the Brillouin zone (BZ), which contains all the inequivalent k vectors closest to the origin of the reciprocal lattice, which has the full symmetry of the reciprocal lattice points that leave the lattice point invariant (point group). For example, in one-dimensional systems the BZ is the $-\pi/a$ to π/a interval. The BZ of the f.c.c. lattice, **2**, is shown in **3**, where some special high symmetry points are indicated by their usual (but alas not very easy to remember) notation. A large portion of most reviews on energy band theory is devoted to the description of the Hamiltonians employed and their properties. Certain features of the calculations

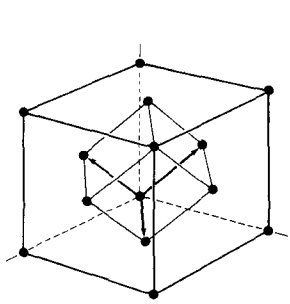

2

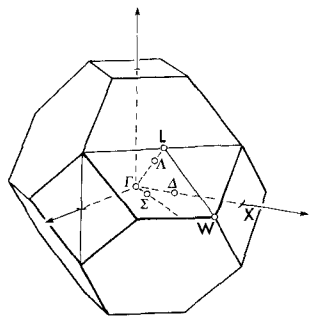

3

remain, however, largely independent of the actual choice of the Hamiltonian. It might be argued that these are precisely the uninteresting results of the calculations. We have adopted another view forced upon us by the fact that these common features of the calculations can be trusted more than particular individual features of the models (such as features which depend, for instance, on certain basis sets or neglects of certain interactions and correlations). The present approach certainly has its limitations, some of which are discussed at the end of this paper.

2. Boundary conditions, density of states

The π-electron system of polyacetylene (**4**), in many regards identical to the simple hypothetical H-atom chain, illustrates well the behaviour of the energy levels as they

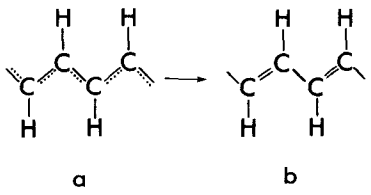

a b

4

form energy bands as the size of the chain is increased. Here every C atom contributes one electron (in a $2p_z$ orbital) to the delocalized π-electron system. Within the Hückel theory for π electrons, the Schrödinger equation (4) is transformed into a matrix eigenvalue equation:

$$\begin{bmatrix} \alpha-E & \beta_1 & & & \\ \beta_1 & \alpha-E & \beta_2 & & \\ & \beta_2 & \alpha-E & \beta_1 & \\ & & \beta_1 & \alpha-E & \\ & & & \cdots & \end{bmatrix} \begin{bmatrix} C_1 \\ C_2 \\ C_3 \\ C_4 \\ \cdots \end{bmatrix} = 0 \tag{7}$$

where C_i are the LCAO coefficients, α and β the Coulomb and resonance integrals, respectively. The energy levels of any finite polyene chain with N carbon atoms has been given by Coulson and Streitweiser (1965) for the $\beta = \beta_1 = \beta_2$ (equivalent bonds) case:

$$\varepsilon_j = \alpha + 2\beta \cos\{j\pi/(N+1)\} \qquad (j = 1, 2, \ldots, N) \tag{8}$$

Let us see what band theory, using Bloch's theorem, would give on this problem. According to (1) the coefficient in (7) can be written as $c_j = \exp(ijk)(1/\sqrt{N})$. The energy eigenvalues are (Coulson and Streitweiser 1965)

$$E_j = \alpha + 2\beta \cos(2j\pi/N) \qquad (j = 1, 2, \ldots, N) \tag{9}$$

The difference between (8) and (9) is due to the different *boundary condition*, because (7) and the open, tend to the same energy level diagram ad $N \to \infty$, and it is customary to the case of *periodic* boundary conditions. In matrix language, this means that instead of (7) we deal with another Hamiltonian, which is supplemented by the matrix element $H_{1N} = H_{N1} = \beta$, making the Hamiltonian cyclic. The 'error' introduced by this boundary condition is small (of the order of $1/N$) for large N. Both models, the periodic and the open, tend to the same energy level diagram, as $N \to \infty$, and it is customary to take the more convenient periodic boundary condition. Figure 1 illustrates the energy level scheme for a small chain, a cyclic larger chain, a linear chain, and an infinite chain. The density of the levels (levels per unit energy interval) will be also given as the density of state diagrams. The latter curves are an alternative representation of the energy level structure to the energy bands. As $N \to \infty$, the k wave-vectors uniformly fill the $(-\pi/a, +\pi/a)$ BZ, continuous energy bands are formed and summations over this zone may be converted into integrals:

$$\frac{1}{N} \sum_k \to \frac{a}{2\pi} \int_{-\pi/a}^{\pi/a} dk \tag{10}$$

Similarly, for three dimension (V is the volume of the unit cell)

$$\frac{1}{N} \sum_k \to \frac{V}{(2\pi)^3} \int_{\mathrm{BZ}} d^3k \tag{11}$$

The $1/N$ factor before the summation ensures that it is normalized as a 'per unit cell' quantity. If n_0 is the number of electrons per unit cell, the highest occupied level, the

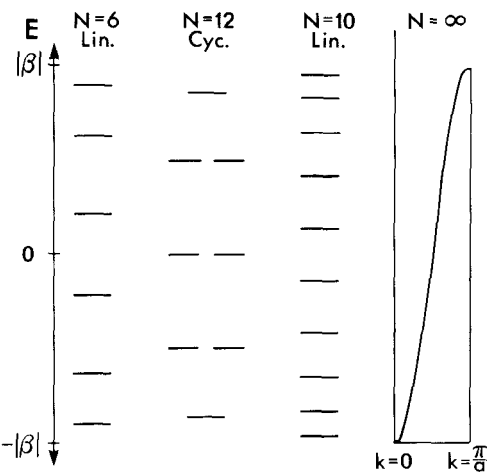

Figure 1. π-Electron energy levels in finite and infinite polyenes.

Fermi level (E_F) is defined by the occupancy sum

$$2\frac{1}{N}\sum_n\sum_k \theta(E_F-\varepsilon_n(k))=n_0 \tag{12}$$

where $\theta(x)$ is the Heaviside function. For metallic systems E_F cuts through one or more energy bands.

One of the features of band calculations, which is new relative to molecular calculations, is the fact that the Bloch functions (1) are complex. However, due to the $\varepsilon_n(-k)=\varepsilon_n(k)$ degeneracy, one can construct the following pair of functions

$$\psi_k^{\pm}(r)=\psi_k(r)\pm\psi_{-k}(r) \tag{13}$$

which are always real, but do not transform according to the irreducible representations of the translation group. The real $\psi_k^{\pm}$ functions may facilitate comparison of solid-state orbitals with molecular orbitals. Even the ψ_k orbitals may be real at some special (high symmetry) points of the BZ, where $\exp(ikR_j)=\pm 1$. For example, such is the case at $k=0$ (termed as Γ point) or in general at (A, B, C) points where A, B and C are equal to either 0, or a half reciprocal lattice vector.

The actual numerical work involved in any one-electron (such as extended Hückel) band structure calculation consists of diagonalizing the k-dependent matrix equation, which is based on (4). If there are m orbitals within the unit cell, the $m\times m$ matrix equations are:

$$\mathbf{H}(k)\mathbf{c}_n(k)=\varepsilon_n(k)\mathbf{S}(k)\mathbf{c}_n(k) \tag{14}$$

giving rise to m $\varepsilon_n(k)$ energy bands where

$$\mathbf{H}(k)=\sum_j \exp(i\mathbf{k}\mathbf{R}_j)\mathbf{H}(j), \quad \text{and} \quad \mathbf{S}(k)=\sum_j \exp(i\mathbf{k}\mathbf{R}_j)\mathbf{S}(j).$$

Here $\mathbf{H}(j)$ and $\mathbf{S}(j)$ are the jth neighbour Hamiltonian and overlap matrices between unit cells separated by the translation vector R_j. For example, for the above given polyene case in equation (7)

$$\mathbf{H}(0)=\begin{pmatrix}\alpha & \beta_1\\ \beta_1 & \alpha\end{pmatrix}, \qquad \mathbf{H}(1)=\begin{pmatrix}0 & 0\\ \beta_2 & 0\end{pmatrix}=\mathbf{H}^{\mathrm{T}}(-1) \tag{14a}$$

if the unit cell is taken to consist of two orbitals (T is for matrix transposition). Larger unit cells are always possible leading formally to more bands and smaller BZs, but usually the smallest possible is chosen. Occasionally it may be convenient to discuss the band structure in terms of a smaller and a larger unit cell, the corresponding BZs are the *extended* and *reduced* zones, respectively. An example may be the case of equidistant polyacetylene, which has one half-filled band, but in discussing its distortion into the alternating structure (**4**) for a comparison it may be convenient to use a reduced zone corresponding to the two orbital per unit cell case. Then, of course, it has formally one filled and one empty band. Other examples for extended zone schemes are given later in this paper.

The knowledge of the energy levels (bands) is the basis for the total energy calculation:

$$E_{\mathrm{tot}}=\sum\sum \theta(\varepsilon_n(k)-E_F)\varepsilon_n(k)+\Delta E \tag{15}$$

where ΔE is the sum of Coulomb, exchange and nuclear–nuclear interactions, neglected in the extended Hückel model. In spite of recent justifications for such an approach (see,

for example, Skriver 1982) caution is in order to keep in mind the limitations of this simple model (see also § 7). In determining the Fermi energy, the DOS curve is usually constructed, which also helps in assessing the important energy regions. Utilization of wavefunction information poses a problem, familiar to practitioners of molecular orbital calculations of large molecules: there are often too many coefficients (in this case also k dependent) to deal with. One way out of this is to concentrate on small regions of the BZ (high symmetry points) which may be important, e.g. due to the closeness of E_F and then concentrate on those orbitals. Alternatively, orbital population contributions from different portions of the BZ may be used to characterize the bonding–antibonding nature of the energy levels. This is done effectively by the energy dependent crystal orbital overlap populations (COOP). These are weighted DOS curves: for the levels in a given energy range the total DOS in that range is weighted by the contribution to the overlap population made by the crystal orbitals in that range (Hughbanks and Hoffman 1983). These curves are negative where the net contribution is antibonding, or positive where the net contribution is bonding in an infinitesimal energy range for a given pair of atoms. Other types of projected density of states curves (PDOS) may display the energy-dependent contribution of a certain type of atomic or orbital population.

An especially useful aspect of these curves is that they enable us to quickly assess the nature of the interactions (bonding or antibonding) between pairs of atoms as a function of electron count.

3. π-Electron systems

3.1. *Electronic structure of polyacetylene*

Let us now turn to a simple one-dimensional example: polyacetylene. This system is a prototype conducting polymer, the subject of intensive experimental investigations (Chiang *et al.* 1979). Owing to its simplicity, it has been a favourite of theoreticians (see, for example, Salem 1963) and it may serve here as a useful model compound to illustrate the effect of lattice distortions on the total energy and the energy gap, as well as the influence of charge transfer on the geometry of the system. We will now show how the nodal structure of the wavefunction at the Fermi energy plays a profound role in determining these properties.

We start by looking at the following simple crystal orbitals for the π electrons of an equidistant *all-trans*-polyacetylene (**5**, **6**, **7**). Using equation (3) it is evident that the corresponding k values are $0, \pi/2a$ and 0, respectively. The energy values corresponding to these wavefunctions are smallest for **5** (all interactions bonding), intermediate for **6** (bonding and antibonding neighbours in equal proportions) and **7** is the most antibonding orbital with the highest energy. Thus, the following band structure is obtained (see figure 2). The degeneracy of **6a** and **6b** is because of the equivalence of the bonds within and outside the unit cell. Once these bonds become inequivalent, as shown in **4**, the intracell bonds become shorter and the intercell ones longer—this has a stabilizing effect on **6a**, and a destabilizing on **6b**. As a consequence a forbidden energy

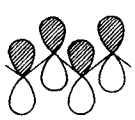

5

6a

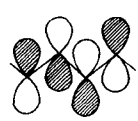

6b

7

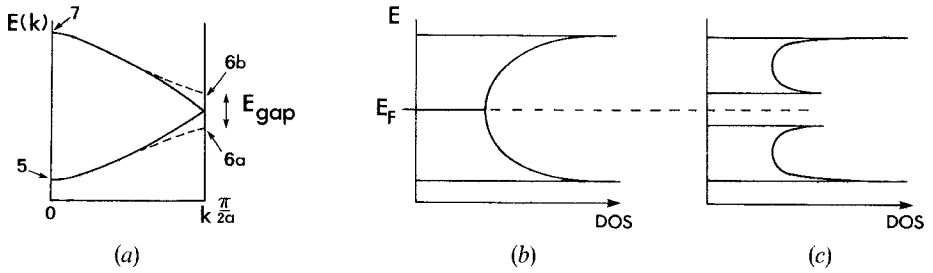

Figure 2. Energy bands of equidistant (——) and alternating (– – –) polyene (*a*). The opening of the energy gap is also illustrated on the density of states curves (*b*, *c*).

gap, E_g, develops as indicated in figure 2(*b*). This driving force leading from a symmetrical structure to a less symmetrical one has its counterpart in the molecular Jahn–Teller distortion. The main difference is that in the present case not only individual levels are moved by the distortion (in an overall stabilizing manner) but a whole fraction of the energy band is tied to the perturbation of the nuclear framework. As a consequence a new pair of singularities occur in the density of states curve for the distorted structure (figure 2(*c*)). The actual wieght carried by this singularity is so large that no elastic force can resist the tendency towards the distortion. Peierls (1955) discovered that any hypothetical one-dimensional metal is susceptible to a metal-insulator lattice distortion and this class of distortions bear his name today. Consequently, when one calculates the total energy as function of the alternation parameter, $\Delta r = r_{C-C} - r_{C=C}$ (keeping their sum constant), the minimum corresponds to $\Delta r \neq 0$. The fact that predictions of this sort are valid for a variety of systems makes the study of the nodal structure of the Bloch functions at and around the Fermi level especially important. Moreover, the effect of charge transfer on the geometrical parameters can be predicted as well.

Figure 3 shows the change of total energy within the EHT model as a function of Δr for a neutral (uncharged) *trans*-polyacetylene chain, as well as for chains with q added charge per cell unit. For $q = 0$ we find that the most stable structure corresponds to non-zero alternation ($\Delta r \neq 0$). The other curves provide us with models for the doped polymer. Positive or negative q means that electrons have been transferred to acceptors or from donors, respectively. In this model the donor or acceptor molecules are structureless, their sole role is to act as sources of *charge transfer*, CT. Thus, the model is a *rigid band model*, we have the same energy band structure for every value of q, the CT parameter, but the occupancy varies with it. The effect on the variation of the calculated $E_{tot}(\mathbf{\Delta r})$ curve is small, as long as $|q| \ll 1$. But as $|q|$ grows, the optimal alternation Δr_{opt} shifts to smaller values, and at a crtical CT value the alternation vanishes: the equidistant configuration is preferred. This comes as no surprise: at $q = +1$ no π electrons are on the chain so there is no driving force for the alternation. At the other extreme, $q = -1$, every bonding and antibonding π state would be occupied and again all bonds must be equivalent.

The crossover from alternating to equidistant chain occurs at around $|q| = 0{\cdot}1$ because only the states in the vicinity of $k = \pi/a$ are active in the Peierls distortion. If these are vacated ($q < 0$) or doubly occupied ($q > 0$) the driving force diminishes. This argument (Kertesz *et al.* 1981) points out the importance of the nodal structure of the one-electron wavefunctions over a small region in k space.

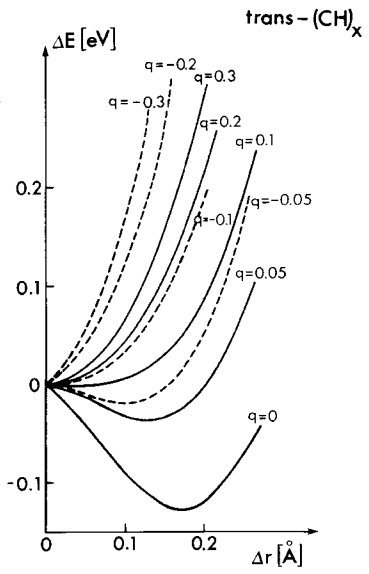

Figure 3. The total energy as function of bond length alternation $\Delta r = r_{C-C} - r_{C=C}$ in *trans*-$(CH)_x$. (after Kertesz *et al.* 1981).

These predictions for the $q=0$ case have been confirmed by powder X-ray experiments (Fincher *et al.* 1982, Lando and Thakur 1984). Evidence for a bond length equalization upon charge transfer is indirect owing to the lack of single crystal samples of doped and undoped polyacetylene.

The general features of the above EHT model calculations are in accordance with other more refined calculations on the undoped and doped models of polyacetylene (see, for example, Kertesz 1982).

3.2. *An analogy between the π-electron systems of doped polyacetylene and graphite*

Both insulating polyacetylene and semimetallic graphite become good electrical conductors upon doping with a variety of donors and acceptors through the formation of intercalation compounds. Although the formation of these compounds is a complex process, its main general feature is that it is accompanied by a charge transfer from or to the carbon π-electron system. One would expect a general π-bond weakening for both signs of the CT, because for $q<0$ (donor compounds) electrons are put to unfilled, usually antibonding levels, while for $q>0$ (acceptor compounds) electrons are taken out from bonding ones. The characteristic feature of many solids, like graphite or equidistant polyacetylene, is that the orbitals around E_F are basically non-bonding, at least in the first-neighbour sense. This is apparent for the latter from the form of orbitals **6** showing that bonding and antibonding neighbours alternate throughout the chain. However, *every second-neighbour interaction* is *antibonding*. As a consequence, this orbital has several features of weakly antibonding orbitals: for $q<0$ (more electrons on the chain) bond weakening, for $q>0$ bond strengthening is expected. Indeed, this assymmetry is observed in the calculations, as illustrated in figure 4, which shows the optimized C–C distances as a function of q.

A similar asymmetric effect for the two signs of the CT has been observed experimentally for graphite compounds (Pietronero and Strassler 1981, Baron *et al.*

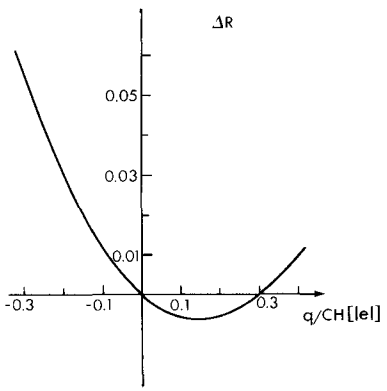

Figure 4. Change of the optimized C–C distance ($\Delta R = R_{opt}(q) - R_{opt}(0)$ as a function of charge transfer, q, in a model of polyacetylene (after Kertesz *et al.* 1981).

1982). We have recently related this asymmetry to that described above for $(CH)_x$ (Kertesz *et al.* 1983, Kertesz 1985).

For this purpose a word or two about the band structure of a graphite layer is in order. The rough results of an extended Hückel calculation are given in figure 5. (The inset shows the BZ.) Of special significance is the K point, at which the highest occupied and lowest empty π bands touch, accounting for the semimetallic behaviour of graphite (Wallace 1947). As often happens in EHT calculations the highest occupied σ bands come out too high. Within the rigid band model electrons are titrated into or from the π orbitals around K. For $q>0$, the σ orbitals at Γ are soon reached and both σ and π electrons are donated to the acceptors. Neglecting these σ orbitals for a moment, the overall pattern of the π orbitals is only pertinent. This is illustrated in figure 6.

The difficulty in a visual representation for these interactions comes from the fact that the Bloch phases are complex. Let us analyse their effect on the total energy. The first-neighbour interactions contribute the terms

$$2\sum(\text{1st neighbours})C_{k\alpha}C_{k\beta}H_{\alpha\beta}=0$$

summing up to zero. However, the second-neighbour interactions result in the energy term

$$2\sum(\text{2nd neighbours})C_{k,\alpha}C_{k,\beta}H_{\alpha\beta}=12\beta''\cos 2\pi/3>0,$$

giving rise to a positive term in the total energy, characteristic of an antibonding orbital. Even though β'' is small, the number of second neighbours is 6 and the resultant effect is not negligible. Figure 7 shows the calculated optimized C–C distance as a function of the CT parameter q, the reference point being the optimized r_{C-C} value for the case without any CT. Two curves are given, one for π-only CT and another for both π or σ CT.

The assymmetry of the π-only curve is a consequence of the antibonding nature of the π orbitals around E_F. In the full $(\sigma+\pi)$ calculations, the high lying occupied σ levels also carry some antibonding character leading to a further weakening of the C–C bonds when they are emptied. Of course, for large values of q the orbitals emptied eventually become predominantly bonding and the curve turns around.

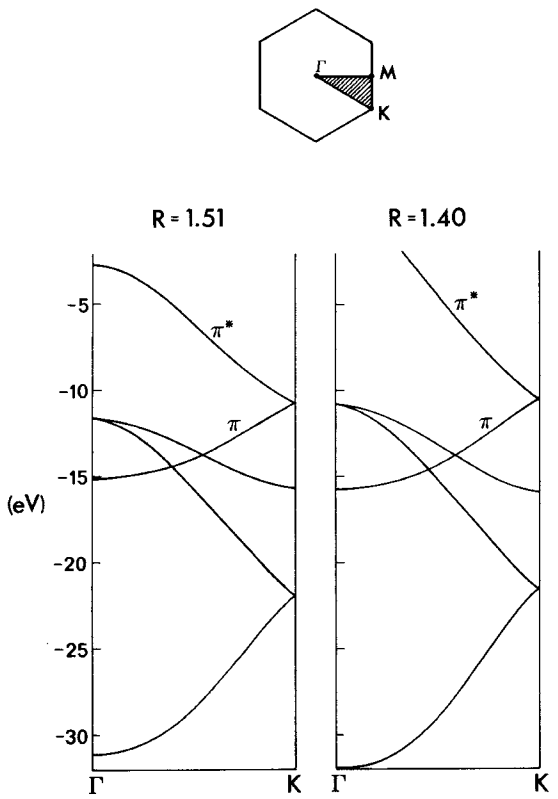

Figure 5. Energy bands of a graphite layer from extended Hückel calculations. (The two band structures correspond to the experimental ($R = 1{\cdot}40$ Å) and the optimized ($R = 1{\cdot}51$ Å) C–C distances, respectively.) The inset shows the BZ of the hexagonal two-dimensional lattice.

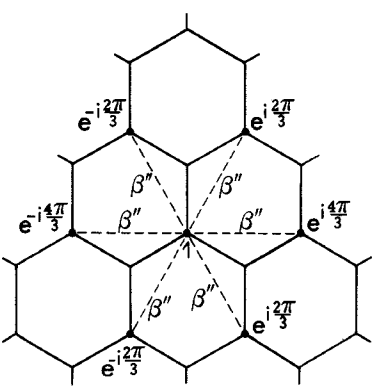

Figure 6. Phase factors in a graphite lattice. β'' is the second-neighbour resonance integral.

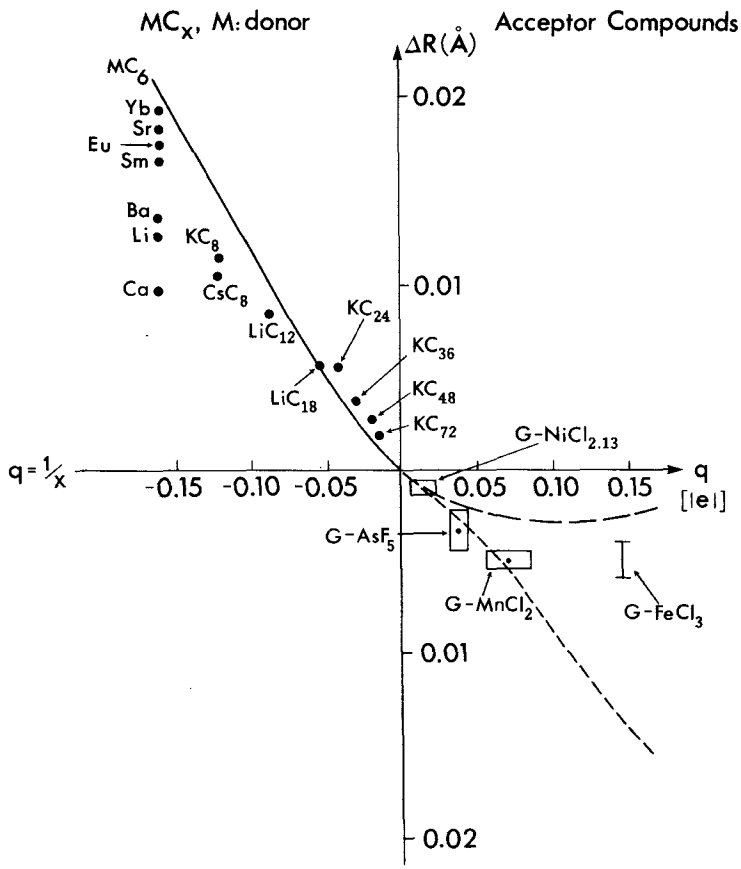

Figure 7. Optimized C–C bond distances in a layer of graphite as a function of charge transfer $[\Delta R = R_{opt}(q) - R_{opt}(0)]$. Experimental data indicated are from Pietronero and Strassler (1981) and Baron *et al.* (1982). For $q > 0$ two curves are given: — — corresponds to π-only charge transfer, while – – – corresponds to π and σ charge transfer.

These results are not only qualitatively, but also—surprisingly enough—quantitatively in accordance with experimental results (Pietronero and Strassler 1981). At this point it is in order to comment on the meaning of the CT parameter, q. While in our calculations it has a clear-cut definition, this is not the case for the experiments. We might—as done in figure 7 for the experimental data—use $1/x$ as a (maximal) measure of q (x occurs in the chemical composition formula MC_x for the first stage intercalation compounds of graphite if M is monovalent). The actual CT will be less. We do not wish to imply that our curves may be used for determining the degree of partial CT in these compounds. The qualitative trends are reasonable enough to substantiate the conclusion that the nodal structure of the wavefunction for graphite has directly measurable consequences in the systematic changes of C–C bonding in its CT compounds.

3.3. *Transition from polyacetylene to graphite*

While polyacetylene has a Peierls-distorted ground state, the structural essence of graphite, the two-dimensional sp^2 carbon layer, has equivalent C–C bonds. It is legitimate to ask how a series of systems of intermediate complexity would behave with respect to bond alteration, i.e. how the passage from $(CH)_x$ to a graphite layer is accomplished. One member of such a series, polyacene (**8**) has recently been studied by Kivelson and Chapman (1983) and Yamabe *et al.* (1982), who concluded that polyacene should have a metallic band structure and that it should *not* undergo a Peierls distortion. This is in contrast with a previous calculation (Whangbo *et al.* 1979) where the band structure of the alternating system (**11**) has an energy band gap and is more stable than the regular structure **8**.

We have examined the π-electron band structure of polyacene, and two further members of the series (**9**, **10**) as well as their tendency to distort (Kertesz and Hoffmann

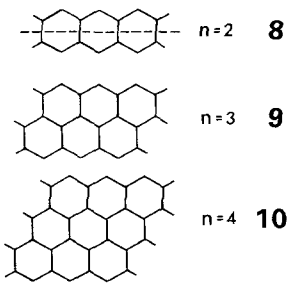

1983). We concluded that the distorted structures with lower symmetry (**11**, **13**) have energy gap openings which decrease sharply with the number of coupled polyacenic chains (n) according to a power law $E_g = C_n(\delta/\beta_0)^n$, where $|\delta/\beta_0| \ll 1$. Consequently, the associated energy gains due to distortion also sharply decrease. Figure 8 reproduces the essential part of the band structure for polyacene.

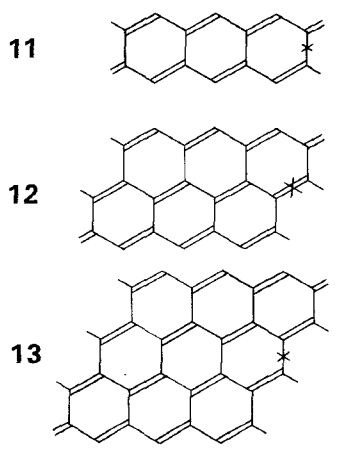

The present discussion is based on lattice sums restricted to second neighbours only, because in the particular systems studied here this restriction enables us to *fully decouple* the π orbitals of the outermost (edge) carbon atoms from the rest of the

orbitals at $k=\pi/a$, as can be seen in **14** for polyacene. This idealization in the summation increases the symmetry of the system. In particular, the decoupling is a consequence of the transverse mirror planes also shown in **14**. This trick of increased symmetry permits a consistent interpretation of the previously published band structures. Due to the decoupling described above, ψ_S and ψ_A become degenerate at $k=\pi/a$ (figure 8(*a*)). Third- (and higher) neighbour interactions lift this degeneracy, by stabilizing ψ_S and destabilizing ψ_A, leading to the crossing in the converged calculation of Whangbo *et al.* (1979) (figure 8(*b*)).

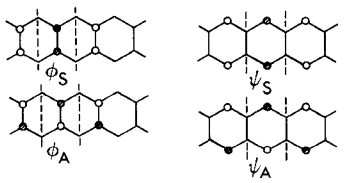

14

The effect of the distortion from the regular (**8**) to the alternating structure (**11**) is to introduce a mixing of ψ_S and ϕ_S as well as ψ_A and ϕ_A. This is because the transverse mirror planes vanish the moment the slightest distortion takes place (Boon 1971). However, the C_2 axes, indicated by a cross on (**11**), still remain a valid symmetry operation. They prohibit the mixing of the A and S states. This new mixing at $k=\pi/a$, absent for the regular structure, stabilizes the highest occupied band states

$$\psi_v=\psi_A+C\phi_A \tag{16}$$

and destabilizes the lowest empty band states

$$\psi_c=\psi_S-C\phi_S \tag{17}$$

leading to a forbidden energy gap, E_g as in figure 8(*c*). Suppose, that the alternation perturbs the resonance integrals by $\pm\delta$. The eigenvalue problem can be solved analytically, giving an energy gap of

$$E_g^{(n=2)}=\beta_0+\sqrt{(\beta_0^2+4\delta^2)}\sim 2\delta^2/|\beta_0| \tag{18}$$

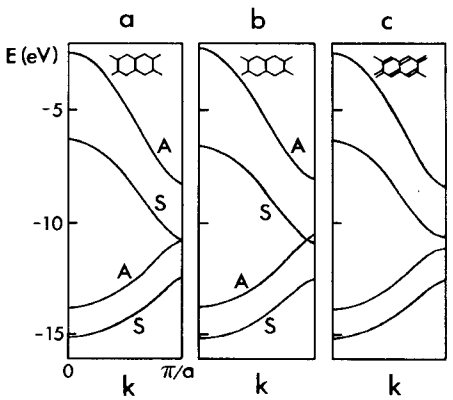

Figure 8. π-Energy bands of polyacene. (*a*) A first-neighbour model calculation, (*b*) a fully converged calculation, (*c*) calculation based on a distorted geometry (Kertesz and Hoffmann 1983).

where an expansion in terms of small $\delta/|\beta_0|$ has been performed. A perturbation calculation yields zero correction at first order, and the same as in (18) at second order (in energy). In case of polyacetylene the gap opening is proportional to the *first* power of the distortion:

$$E_g^{(n=1)} = 4\delta \tag{19}$$

This is due to the direct coupling of the degenerate states at $K = \pi/a$ to the lattice deformation, as illustrated in (**6a**) and (**6b**).

The one-dimensional polymers (**9**) (polynaphthene, let us call it poly-C_6) and (**10**) (polypyrene, let us call it poly-C_8) are further members of a series that makes an obvious transition to two dimensions. The symmetry adapted wavefunctions of $k = \pi/a$ for poly-C_6 are illustrated (**15**). The following crystal orbitals are obviously degenerate pairs:

15

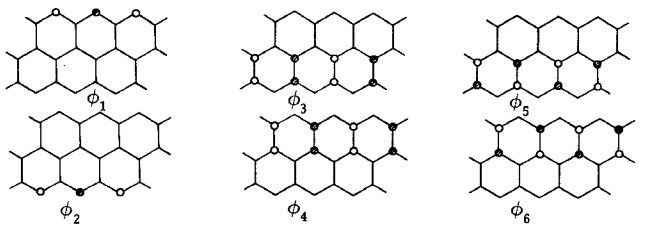

(ϕ_1, ϕ_2); (ϕ_3, ϕ_4); and (ϕ_5, ϕ_6). ϕ_1 and ϕ_2 lie at the Fermi level. The deformation from the regular to the distorted (**12**) structure introduces a coupling between the edge atoms of ϕ_1 and ϕ_2, giving rise to a splitting. The lack of mixing of ϕ_1 orbitals of the same symmetry is due to the restriction of the second-neighbour approximation model. ϕ_1 is decoupled from ϕ_4 and ϕ_6 because of this, while it does not interact with ϕ_2, ϕ_3 and ϕ_5 due to the vertical mirror planes and the changes of signs that arise as a consequence of being at $k = \pi/a$. The distortion switches on some coupling. The new symmetry adapted wavefunctions will be the $\psi_i - s$: $\sqrt{2}\psi_{1,2} = \phi_1 \pm \phi_2$, $\sqrt{2}\psi_{3,4} = \psi_3 \pm \phi_4$ and $\sqrt{2}\psi_{5,6} = \phi_5 \pm \phi_6$. These are still degenerate for the undistorted system. In the distorted system ψ_1 interacts with ψ_3 and ψ_5, leading to a stabilization of it by $E_g/2$, while ψ_2 rises by the same amount due to mixing with ψ_4 and ψ_6. The Hamiltonian for the distorted system at $k = \pi/a$ in terms of atomic orbital coefficients is

$$H = \begin{bmatrix} 0 & \delta & & & & \\ \delta & 0 & 1 & & & \\ & 1 & 0 & \delta & & \\ & & \delta & 0 & 1 & \\ & & & 1 & 0 & \delta \\ & & & & \delta & 0 \end{bmatrix} \tag{20}$$

A perturbation calculation for small δ yields

$$\psi_1' = \psi_1 + a\psi_3 + b\psi_5, \qquad \text{with } a = -b = -\delta/\beta_0\sqrt{2} \tag{21}$$

therefore, even at second order in energy a cancellation occurs. The first non-zero term for $E_g^{(n=3)}$ is third order in energy:

$$E_g^{(n=3)} = 4\delta^3/\beta_0^2 \tag{22}$$

in a similar way for poly-C_8 it can be shown that

$$E_g^{(n=3)} = \text{const}\,\delta^4 \tag{23}$$

These calculations have demonstrated that the first-order (linear) Peierls gap opening is absent in carbon chains with two or more coupled polyenic chains, due to the idealized symmetry of the systems. However, a higher-order gap always occurs:

$$E_g^{(n)} = C_n(\delta/\beta_0)^n\beta_0 \tag{24}$$

driving the lattice to distort. We have termed this effect as the higher-order Peierls instability. Actually, $\delta/|\beta_0|$ can be realistically estimated to be about 0·2 or less. ($\delta/|\beta_0| = 0{\cdot}135$ for a distortion of 0·08 Å, a value close to the experimentally observed distortion for polyacetylene (Fincher *et al.* 1982).) Thus, the higher-order gaps will be much smaller than the linear gap of polyacetylene, which is about 1·4 eV (Fincher *et al.* 1978). As a consequence even small interchain effects may actually stabilize a metallic state in such systems, in sharp contrast to the linear Peierls system of polyacetylene. This actually happens in graphite ($n \to \infty$), which has $E_g = 0$ and a regular structure, and not a distorted one.

The above simple considerations (Kertesz and Hoffmann 1983) qualify Peierls theorem on the intrinsic instability of one-dimensional metallic systems, and have a broader applicability. The high-order Peierls gap openings described in this section may occur in other systems as well, where chains susceptible to first-order Peierls distortion are not weakly coupled together, forming more complicated quasi-one-dimensional semimetallic systems (see, for example, $(SN)_x$ below).

4. Further one-dimensional examples

Distortions similar to the one observed for polyacetylene, preventing an ideal structure with metallic bandstructure to occur, are quite often found in the recent quest for synthetic metals. Their theoretical study is partly motivated by efforts to find ways to stabilize the ideal, metallic structures.

4.1. *A Peierls-dimerized chain: tetramethyldistibolyl*

The crystal structure of 2,2′,5,5′-tetramethyldistibolyl (**16**) reveals the presence of an alternating chain of short and long Sb–Sb contacts. Band structure calculations have been performed for the experimental, as well as for an idealized, equidistant metallic chain by Hughbanks *et al.* (1982). (The methyl groups have been replaced by hydrogens, as is usual in this trade.) Because of the interactions between the Sb atoms along the chain the planes of the $Sb(C_4H_4)$ units are not symmetry planes. Thus, the p_z

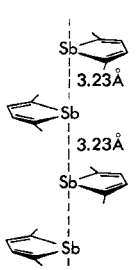

16

and n_z orbitals will mix, producing a degenerate pair of orbitals indicated in the r.h.s. of the band structure in figure 9.

A Peierls-type dimerization distortion follows from the stabilization of the lower one of the pair: bonding combination of the orbitals becomes shorter, antibonding longer. This band structure may also serve as an illustration of the *extended zone scheme*. The elementary cell in the regular or alternating structures contains two Sb (C_4H_4) units. However, the structure of the matrices expressing the interactions between these units cannot tell whether it is a pure translation or a screw axis of rotation which connects the neighbouring unit cells (for a more complete discussion of screw axis in polymeric electronic structure see Blumen and Merkel (1977) and Bozovic and Delhalle (1984)). Therefore, the band structure can be represented using an effective elementary cell of only *one* Sb (C_4H_4) unit in the non-dimerized case. The corresponding energy band structure is shown in figure 10.

This figure reveals that there are not really as many band crossings as it might appear from figure 9, but rather several crossings are derived from the 'backfolding' of the band structure of figure 10 to that of figure 9. Otherwise, the splitting of the degeneracy at E_F leads to a sizeable energy gap and energy gain stabilizing the dimerized structure, which explains the experimentally found geometry and optical absorption.

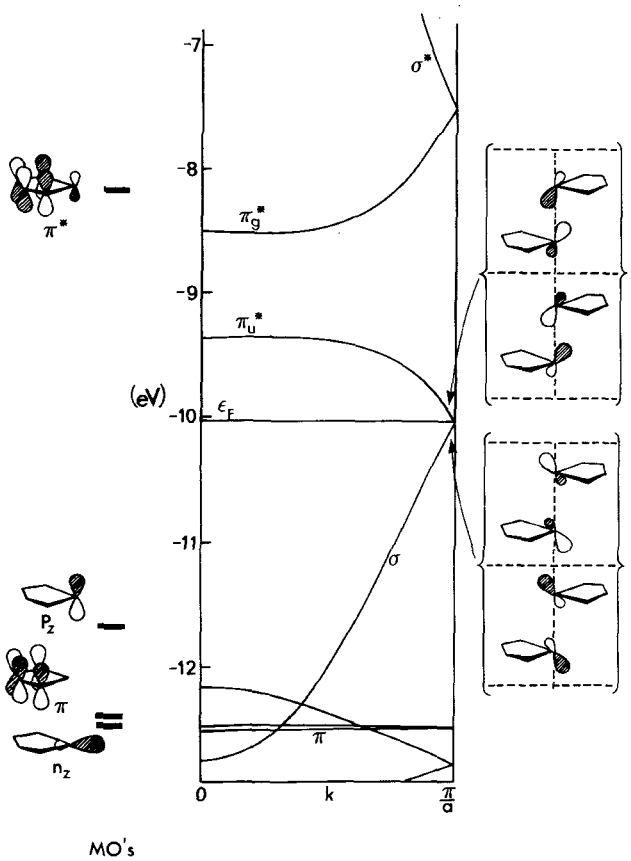

Figure 9. Energy bands of a tetramethyldistibolyl chain (molecular orbitals of the chemical unit cell are indicated on the left) (from Hughbanks *et al.* 1982, with permission).

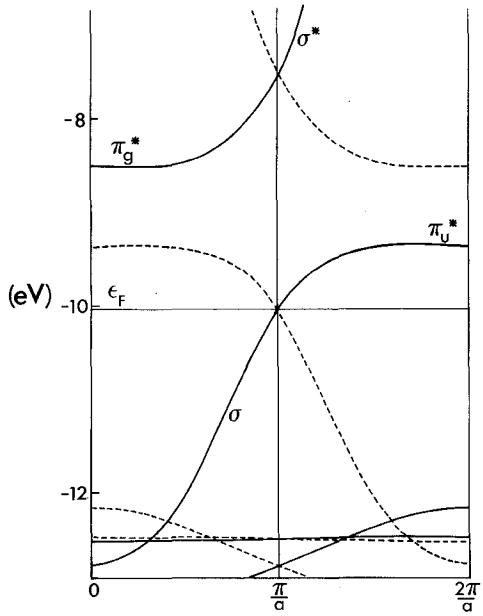

Figure 10. Energy bands of figure 9 in a reduced (backfolded) BZ (from Hughbanks *et al.* 1982, with permission).

4.2. *A chain with two-thirds-filled band: polyiodide,* $(I_3^-)_x$

Two of the structures discussed above were derived as dimerized chains resulting from a Peierls distortion of a half-filled ideal metallic chain. Other partial fillings lead to larger aggregations of atoms. For example, polyiodide chains of the $(I_3^-)_\infty$ or $(I_5^-)_\infty$ type can be derived (Kertesz and Vonderviszt 1982) as Peierls-type distortions of two-thirds-filled or three-fifths-filled σ bands of an ideal metallic polyiodide chain. We will show here the arguments for the two-thirds-filled case only. A two-thirds-filled band of χ atomic orbitals has the following crystal orbitals at the Fermi level

$$\psi_{1,2} = \frac{1}{\sqrt{N}} \sum_j \exp[i(k_F)_{1,2} j a_\chi] \, \chi(r - ja) \tag{25}$$

where $(k_F)_{1,2} = \pm 2\pi/3a$. These orbitals being complex, their nodal structures are not immediately as suggestive as for the half-filled band case as **6a** and **6b** are. The two orbitals, (25), are degenerate, and only one is filled in the two-thirds-filled band case. There is a Peierls-type driving force towards a nuclear deformation of the lattice if an energy band gap results from it which is linear (first order) in the distortion. This condition is fulfilled if the distortion has the periodicity of $(2k_F)^{-1}$, causing a periodic lattice potential:

$$V(r) = V_0 \cos(2k_F r) \tag{26}$$

In our case this leads to the following perturbation theoretical (PT) result ($H = H_0 + V(r)$ is the Hamiltonian modified by the nuclear distortion). Suppose that the two (degenerate) states are ψ^{k_F}, and ψ^{-k_F}. Then using $V(r)$ in degenerate PT one obtains a splitting of these two states by $\pm V_0$ and the corresponding states will be

$$\psi_\pm = 1/\sqrt{2}(\psi^{k_F} \pm \psi^{-k_F}) \tag{27}$$

These new states are purely real, signalling that the new BZ edge due to perturbation (26) is now at $\pm k_F$. The patterns of the iodine 5*p* orbitals for the two degenerate real orbitals are shown as insets in figure 11. These will be shifted downwards or upwards following the trimerization distortion, leading to energy stabilization favouring a structure with (I_3^-) units. The band structure is illustrated in figure 11. The actual calculations show a more complex picture, because the 5*p* orbitals' hydridization with 5*s* is not negligible. A large number of solid-state compounds enclose polyiodide chains, and the experimental data on their structural and electrical properties could be rationalized using the orbital arguments above.

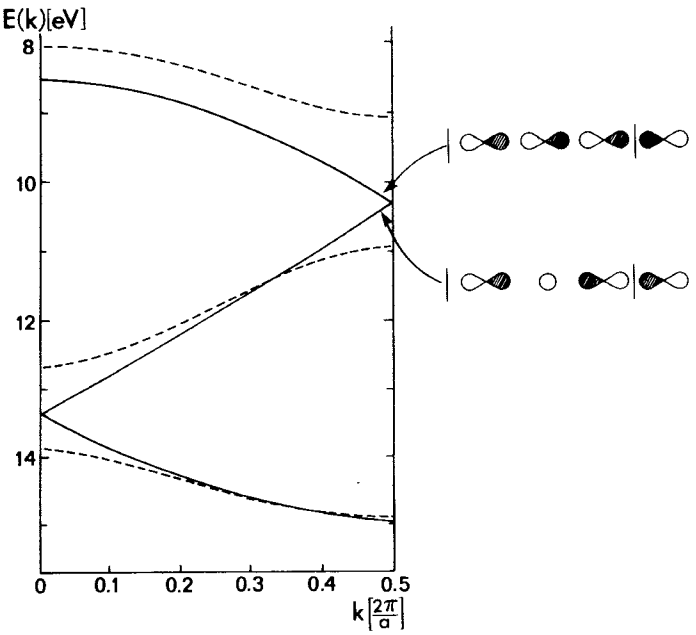

Figure 11. σ-Energy bands of an infinite $(I_3^-)_\infty$ chain, with regular (——) and trimerized geometry (– – –). The insets show the nodal structure of the orbitals, which are relevant in the Peierls distortion (after Kertesz and Vonderviszt 1982.)

4.3. *Polysulphur nitride: a 'chain' with a three-quarters-filled band which does not distort*

Polysulphur nitride has metallic properties and consists of chains packed closer than van der Waals interactions, as shown in figure 12 (Cohen *et al.* 1976). Neglecting these weaker interactions, the planar chain has 6π electrons per S_2N_2 units: formally a three-quarters-filled π-band case. This would be susceptible to a Peierls-type distortion to a lesser degree than polyacetylene for two reasons. First, the $2k_F$ periodicity encloses four atoms (two SN units) in contrast to the two CH units in polyacetylene. This means that the required distortion is spread out over four atoms and no simple bond length alternation pattern could occur, as different bond distances would change smoothly from bond to bond along the chain. The other, more important, factor preventing $(SN)_x$ from a metal to insulator transition is due to its relatively strong interchain interactions, which cause the band structure to split as is shown in figure 13.

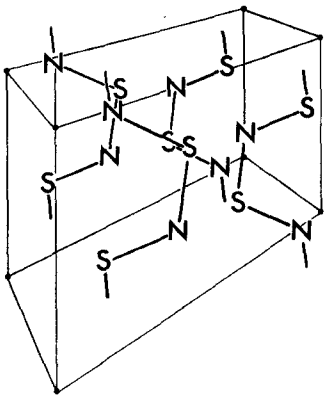

Figure 12. Crystal structure of polysulphur nitride, $(SN)_x$ (after Cohen *et al.* 1976).

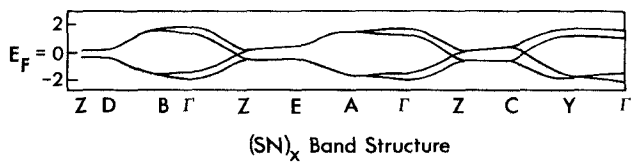

$(SN)_x$ Band Structure

(*a*)

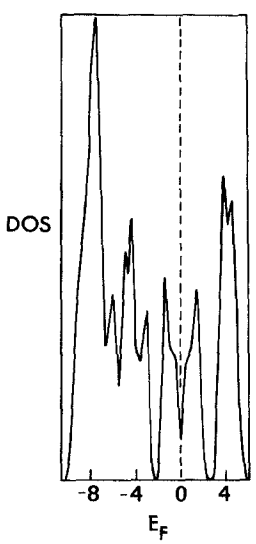

(*b*)

Figure 13. (*a*) π-Electron bands of $(SN)_x$. (*b*) The calculated density of states (*E* in electron volts) (after Batra *et al.* 1977).

The presence of a deep DOS valley at the Fermi level is a manifestation of the three-dimensional interchain coupling, which gives rise to the doubling of the bands along ΓZ. (The BZ is given in the original papers.) The Fermi level is thus moved from the Z point (Z is the endpoint of the one-dimensional BZ, where the Peierls gap opening would occur) to the vicinity of the crossing points (Friesen *et al.* 1975). The energy levels near E_F are found only in the immediate vicinity of the crossings of these bands, of which there are actually two. Such regions—and this part of the argument is general—constitute only a very small fraction of the three-dimensional BZ, thus the DOS becomes very low around this crossing. In contrast to this, for a one-dimensional system, like an $(SN)_x$ single-chain model, the DOS is much larger because here it is proportional to the ratio of the length of a small k increment near Z to the length of the whole BZ, $2\pi/a$, and the length fraction is much larger than the volume fraction for the three-dimensional case. Consequently, the three-dimensional nature of the bands pushes levels *away* from E_F. This makes the system 'less' metallic, but at the same time less susceptible to a Peierls-like distortion, which is based on the effectiveness of pushing levels away from the Fermi level by way of a geometrical distortion.

The discussion above (Ching *et al.* 1977) explains how three-dimensional couplings may suppress the Peierls distortion in $(SN)_x$, which indeed, has metallic properties (Street and Clarke 1980). Details of the published band structures vary significantly, but the dip of the DOS around E_F discussed above is one of those essential general features invariably found in the calculations, which we emphasize in the present review.

5. Two-dimensional examples

5.1. *Charge transfer in graphite*

Intercalated layer compounds of graphite exhibit a wide variety of unusual electrical, optical and magnetic properties. The rigid band model (in which electrons or holes are 'titrated' into the unrelaxed energy bands of the host) is successful in accounting for some orbital controlled structural trends discussed above. However, in metal–graphite intercalation compounds, the interplanar host distances seem to correlate with the ionic radii, while the guest–guest distances correlate more with the metallic radii. Table 1 shows a selection of such data.

This inconsistency implies some degree of metal–metal bonding, partly through the carbon $2p_z$ (π) orbitals, giving rise to a partial localization of the transferred charge. This explains some of the discrepancies between the chemically defined CT, f_{chem}, and the physically defined CT, f_{elec}, as described by Fisher (1980). Band-structure calculations on fully doped alkali metal graphites reflect such localization of some of the transferred charge (Holzwarth 1983). The hybridization of these $2p_z(\pi)$ states with

Table 1. Ionic and atomic radii, and geometrical dimensions of some selected metal–graphite compounds (in angstroms)†.

	LiC_6	CsC_8	BaC_8	SmC_6	YbC_6
Metallic radius	1·53	2·67	2·22	1·81	1·94
M–M in-plane distance/2	2·13	2·46	2·46	2·13	2·13
Ionic radius (Li^+, Cs^+, Ba^{2+}, Sm^{2+}, Yb^{2+})	0·60	1·69	1·35	1·04	1·13
Thickness of C–M–C layer	3·74	5·94	5·28	4·58	4·57

† Data from Herold (1981) and Hulliger (1976).

intercalant orbitals have been used to interpret inversed photoemission data (Fauster *et al.* 1983). Hybridization of Li 2*s* and carbon π electrons had been found in LiC_6 both theoretically and experimentally (Wertheim *et al.* 1980). The proximity of the $2p_z(\pi)$ carbon orbitals to the intercalant layers permits them to 'back-donate' some of the transferred electrons, providing the basis for unique metallic bonding between the guests, assisted by the presence of the delocalized host electrons. In this sense there is a limit as to how far the concept of charge transfer can be pushed. After all, the division of the charge distribution into atomic regions is as arbitrary for solids as it is for molecules.

5.2. *Layers of transition metal dichalcogenides*

Among the two-dimensional systems, an interesting prototype structure is that of the transition metal chalcogenides, MX_2, X = S, Se, Te. There is one fundamental aspect of the structure that varies systematically through the transition series (see Wilson and Yoffe 1969). The two chalcogenide layers forming a slab can be stacked directly above each other, making trigonal prismatic holes for the metals. Alternatively, the layers may stagger, forming octahedral holes. The IVB metals all have octahedral structures. For VB metals most have octahedral, some trigonal prismatic geometries, and for VIB the reverse is true. In group VIIB we again find octahedral structures, albeit distorted ones.

Band structures and total energies of the two different kinds of layers, trigonal prismatic versus octahedral, have been compared (Kertesz and Hoffman 1984 a) using a *rigid band model*, i.e. by using the very same band structure for different compounds across the Periodic Table. The study of such an *average band structure* is necessarily not accurate in its details, and for the individual compounds a number of band structures have been compiled which compare more favourably with experiments concerning the individual systems (see, for example, Mattheiss 1973). On the other hand, the rigid band model is, as we shall see, capable of accounting for the octahedral–trigonal prismatic–octahedral trend as one moves across the transition series as the *d* electron count changes. Since there are no bonding X–X contacts in these dichalcogenides we can assign formal oxidation state II to X, reaching oxidation state IV for the metals in MX_2.

In addition to the *d* electron count variation across the series, packing ought to be considered as well, but here we focus solely on the electronic aspects. A strong argument for an electronic rationale for the choice between structural alternatives is to be seen in the observation that compounds choose between one and the other structure while having the same ionic sizes.

We shall first look at the band structures of the ligand systems only, free of the metal. We anticipate some differences due to the different packing. Both layers are hexagonal, with the BZ shown in figure 5. The unit cells of the two two-dimensional layers are shown in **17** and **18**. The upper portions of these illustrate the trigonal prismatic and the octahedral environments, respectively.

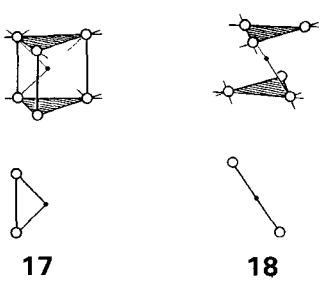

17 **18**

The dark dot indicates the eventual position of the still absent metal, and the lines the M–X axes. There is a twofold symmetry element in both cases, but it is a different one for the two structures—a mirror plane σ_h for the AA double layer, an inversion centre *i* for the AB structure. Significant for the subsequent discussion is the fact that the nearest interlayer X–X contact is within one unit cell for AA, **17**, but between two different cells for AB, **18**.

Let us slowly build up the band structure of the two layers, taking Se as an example. Each Se enters with a 4*s* and three 4*p* levels. The choice of axes will be such that p_z will be perpendicular to the layer.

At the Γ point we expect two *s*(Se 4*s*) bands, symmetric and antisymmetric with respect to σ_h or *i*. The splitting should be slightly larger for AA. At the same Γ point in-plane $4p_x$ and $4p_y$ levels (four altogether) will be pushed up, because of in-plane interactions (see **19**, **20**). While the interaction of centre 1 with 2 (numbering given in **19**)

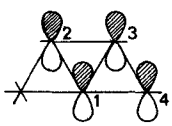

19

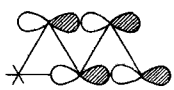

20

and 1 with 3 is antibonding, 1–4 is only weakly bonding. The other in-plane orbital, **20**, degenerate by symmetry with **19**, is 1–4 strongly antibonding, which dominates the character of this orbital. Then the **19**–**20** pair may be bonding or antibonding across the two layers, giving rise to a small splitting.

The $4p_z$ orbitals are not interacting strongly in-plane, for X–X π interactions, **21**, at a non-bonding separation between chalcogens, are weak. But the $4p_z$ orbitals will split into bonding and antibonding combinations due to interlayer interactions. The two (bonding and antibonding across the layers) combinations are illustrated schematically in **22**–**24**. Note that the splitting is formally due to interunit-cell interactions in **22** and **23** but intracell interactions in **24**. Physically, the interaction is similar—it is expected to result in a substantial splitting, greater for the AA case where the overlaps are larger along the *z* direction.

The case of the *K* point is quite different. Now, due to Bloch's theorem, a phase factor is associated to every translation. This factor is $\exp(i\phi)$, and $\exp(-i\phi)$ $(\phi = 2\pi/3)$

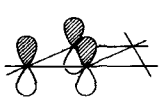

21

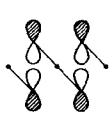

22

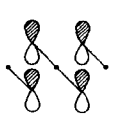

23

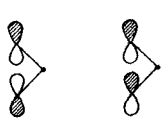

24

for one in-plane lattice vector translation, if they are chosen at 60° with respect to each other. As a consequence, certain degeneracies present in the AB (octahedral) system are lifted in the AA one. We will illustrate this for the AB octahedral hole case through the top view of the two combinations, **25** and **26**. The numbers on the atoms are proportional to the atomic orbital coefficients ($4p_z$ or $4s$).

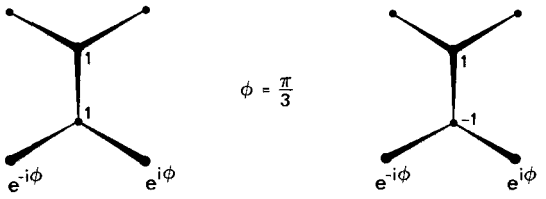

25 **26**

Orbitals **25** and **26** are degenerate, as are the $2p_z(\pi)$ orbitals of a single graphite layer at the K point in its BZ (Wallace 1947). This can be seen most easily by examining the 'bond order' or overlap population around the lower atom in these orbitals. The 1, 1 combination in **25** contributes a 'bond order' of 1 to the overlap population, while the $1, \exp(i\phi)$ and $1, \exp(-i\phi)$ combinations are each antibonding with 'bond order' $-1/2$ each. The sum is zero. The sign if each contribution changes in **26**, but the total is still zero.

In the AA packing the symmetry is lower, this degeneracy is absent and the splitting is directly related to the interplane bonding–antibonding interactions. The in-plane $4p_x$ and $4p_y$ orbitals at K are slightly bonding, and their splittings due to interlayer separations are small again.

Summarizing the general features of the two chalcogen layers' energy level scheme for these two high symmetry points we obtain **27** for the octahedral and **28** for the trigonal prismatic case.

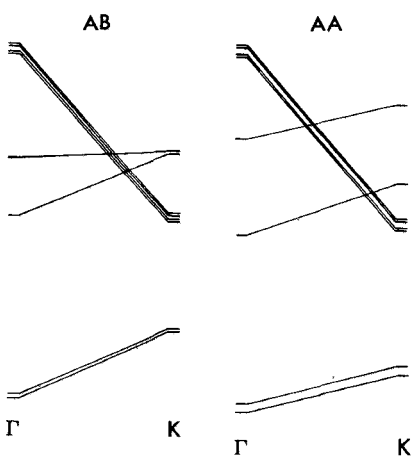

27 **28**

The actual computed band structure is shown in the paper by Kertesz and Hoffmann (1984). Several necessarily avoided crossings occur along the route from Γ to *K*, but the general trends are precisely those discussed above.

We proceed directly to the MX_2 structures by filling every octahedral hole of the AB layer with a transition metal M, and every second trigonal prismatic hole of the AA layer. The specific metal chosen is Re, and X is Se. The resulting band structures are shown in figure 14.

Let us look at the general features of these band structures. The *p* bands of either AA or AB layers of chalcogenides lie between −10·5 and −16·5 eV. The resonance with Re 5*d* levels, placed at −12·66 eV, is excellent, as is the overlap between Re and its six neighbour Se atoms. Thus there is substantial Re–Se interaction, splitting the Re *d* block: the effective crystal field at Re is large. In the band structures of figure 14 we see two Se *s* bands at low energy, pushed down only a little from their metal-free positions. Above these are six bands, largely Se *p*, then three bands in the region between −9 and −13 eV which are largely Re *d*. These are a set of three below two, and the Fermi level in the real dichalcogenide structures, electron counts d^0–d^6, will be in this region. The composition of the various bands is derived from projections of the DOS, shown in figure 15.

The stability of the layered structure becomes small for electron counts over d^3, according to experience, and other (pyrites, marcasites) structures are observed for the VIIIa group dichalcogenides, for instance. Although we do not attempt to compare the MX_2 structures with these three-dimensional structures, it is worth looking at the crystal orbital overlap population (COOP) curves displayed in figure 16. (The trend for octahedral and trigonal prismatic is very similar.) Above −11 eV there is a negative peak for all three types of bonds (M–M, X–X and M–X) indicating that filling much over this level destroys the structure, as such. Also apparent is the dominating bonding character of the M–X bonds up to ~ −13 eV. The M–M bonds are weak, and start to pick up some antibonding contribution in the middle of the *d* bands (at around

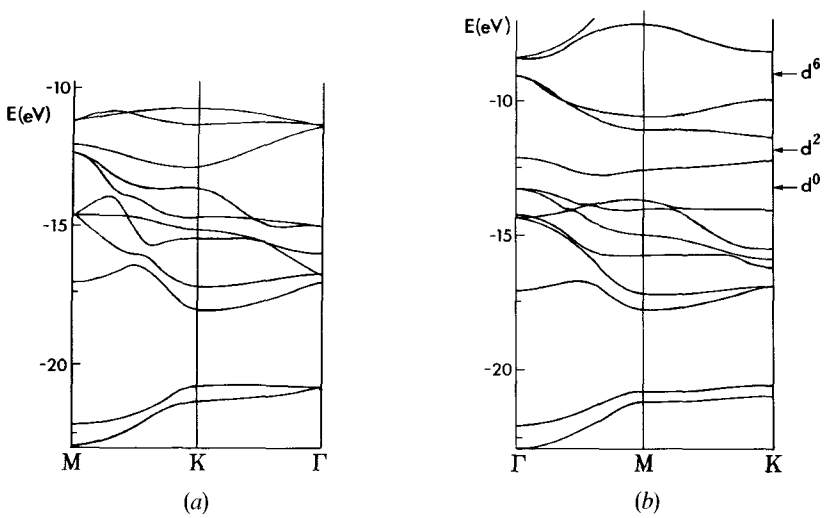

Figure 14. Energy bands of an octahedral (*a*) and a trigonal prismatic (*b*) transition metal dichalcogenide layer.

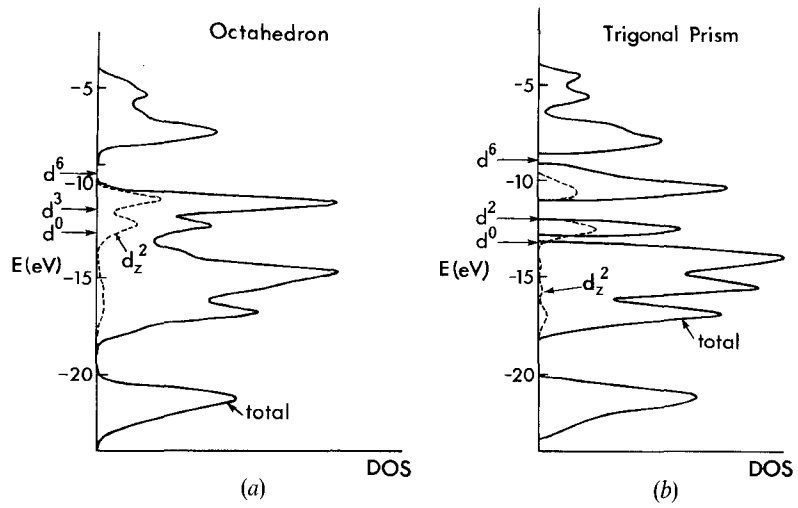

Figure 15. Density of states for an octahedral (*a*) and a trigonal prismatic (*b*) layer (based on bands on figure 14).

-14 eV). The X–X bonds' first significant antibonding contribution from below is at ~ -15 eV, a rather low value, which is in the middle of the in-plane bands of the metal-free ligands' bands. Thus, the orbitals around the Fermi level for all d^0–d^6 electron counts are antibonding for X–X.

For a d^0 electron count, bands 1–8 in figure 14 are filled, there is little difference in total energy between the trigonal prismatic and octahedral layering, even though the details of the bands differ. There are significant differences at Γ and K for the crucial bands 9, 10 and 11. At Γ bands 10 and 11 are shifted up in the trigonal prism relative to the octahedron. In the latter geometry the centre of symmetry prevents one Se $p_{x,y}$ combination (**29**) from interacting with a d orbital, thus keeping its energy down. In the trigonal prismatic environment both $p_{x,y}$ combinations, **30** and **31**, can interact with d orbitals.

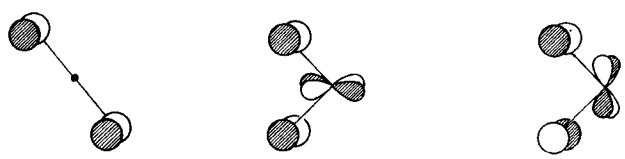

29 **30** **31**

At K the differences can be traced to the same symmetry lowering factor that in the metal-free bilayer produced a substantial splitting in the trigonal prismatic arrangement. Band 9 goes down, band 11 up, relative to the octahedron.

As we gradually fill these bands, first the trigonal prismatic geometry will become relatively more stable, due to the downward shift of orbital 9 at K. This effect reaches its maximum around d^2, when an opposite trend starts, and the octahedral structure will start to become more stable, due to the upward shift of bands 10 and 11 at Γ and at K. Figure 17 depicts the total energy differences as a function of the d electron count.

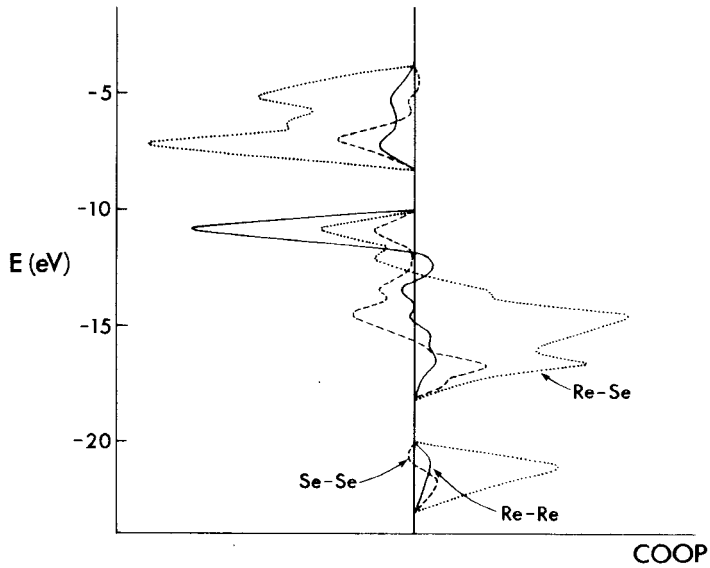

Figure 16. Crystal orbital overlap population (COOP) for Re–Re (——), Re–Se (– – –) and Se–Se (· · ·) bonds in an octahedral $ReSe_2$ model. Above −11 eV ($\sim d^3$ filling) all three kinds of bonds become strongly antibonding.

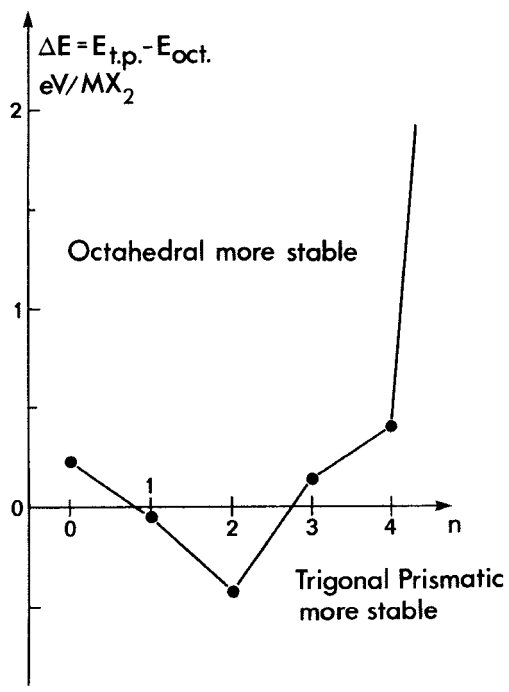

Figure 17. Relative stability of octahedral and trigonal prismatic coordination in an MX_2 layer. Connecting lines provided to guide the eye (after Kertesz and Hoffmann 1984a).

The curve reflects the trend in agreement with the experimental findings. Most notably this correlation is independent of the actual atomic parameters and the radius ratios. We have an electronic effect at hand, a consequence of the symmetry-controlled band structures at Γ and K.

Comparison of the energetics of different related solid-state structures as a function of electron count is a great subject of its own. Several studies of this kind have been reported: for example, Pettifor (1977) has interpreted the structural trends in elemental transition metals, Burdett and Lee (1984) have studied the structure of AB alloys and Burdett and Hughbanks (1984) the structural trends in early transition metal monoxide defect structures, just to mention a few. Burdett (1984) has recently related the general shapes of the energy differences of two structures as function of the electron counts to topological connectivities of the related lattices. It appears that, other factors being equal, connectivity and electron count largely determine the stability of a structure over alternative structures. Extended Hückel theory provides an ideal model for such cases, as it most effectively simulates the constancy of the environments. Several beautiful examples are reviewed by Burdett (1984).

5.3. *The clustering distortion in $ReSe_2$: a Peierls distortion?*

The actual structure of $ReSe_2$ (Alcock and Kjekshus 1965) can be viewed as a distorted ideal octahedral MX_2 layer compound. The distortion leads to formation of diamond-shaped Re_4 units chained together to form quasi-one-dimensional arrays, as illustrated in **32**. Is this a consequence of a Peierls-like distortion?

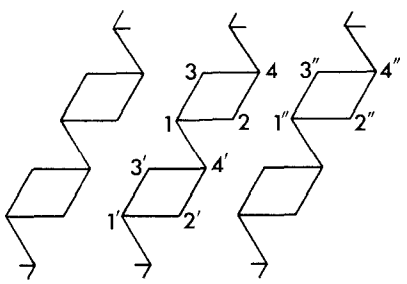

32

The unit cell of a two-dimensional layer-model as a consequence is Re_4Se_8, with 76 valence electrons filling 38 orbitals on average over the BZ. Our starting point will be the undistorted band structure, which will be first 'backfolded', i.e. derived from the $ReSe_2$ band structure. The new unit cell (Re_4Se_8) is four times larger than that of the undistorted one, thus the new BZ is one-quarter of the original one, as illustrated in **33**.

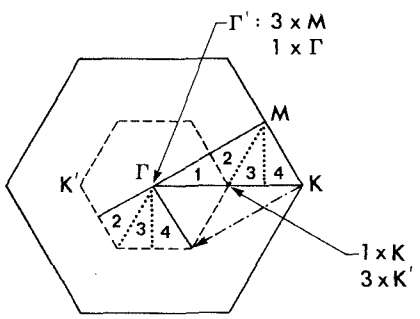

33

The primed high symmetry points refer to the new, small zone, while those of the old, four times larger, are unprimed. Regions 1–4 are inequivalent in the old zone, but are mapped to region 1 in the new zone.

A number of new degeneracies occur at the new special points. These become important because after distortion takes place some of the levels split strongly, in fact driving the distortion electronically. The new bands can be pieced together, from the previous band structure of the undistorted system, using the mappings indicated in **33**. One such piecing-together process is illustrated in figure 18.

In Re_4Se_8 12 electrons have to be put into these bands (d^3). Of particular importance around the Fermi level are the triply degenerate bands (originating from M) and the doubly degenerate ones (originating from Γ), in the Γ' point bands 37–41. Likewise, important around the Fermi level are the doubly degenerate bands 37 and 38 originating from K, and the triply degenerate levels (39, 40 and 41) originating from K', in the K' point. These levels are derived from bands 9–11 of figure 14(*a*), and have predominant $d_{x^2-y^2}$ and d_{xy} (in-plane) character and thus will be strongly affected by an in-plane distortion in which metal–metal overlaps are turned on. To put it another way, these in-plane bands will drive the distortion, if possible trying to open up a substantial band gap at the Fermi level.

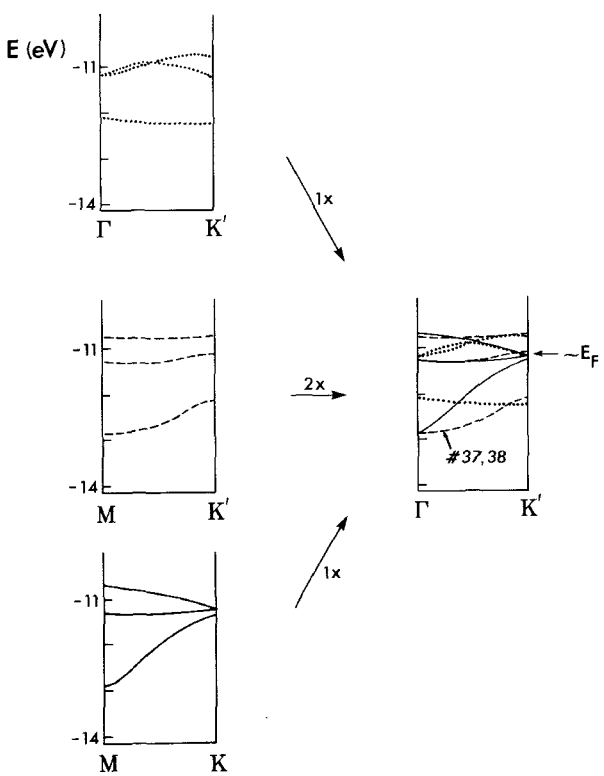

Figure 18. *d* Bands along Γ to K' line in the reduced (backfolded) BZ, **33**, for undistorted Re_4Se_8. (——) originates from M to K, (···) from Γ to K' and (– – –) from M to K' (twice). The band structure is derived from that of $ReSe_2$ (undistorted) (after Kertesz and Hoffmann 1984 a).

Let us examine the detailed splitting of these bands as the distortion develops. In the Γ point band 39 is expected to be perturbed upwards, 40 downwards and 38 to remain at an intermediate energy. This is indicated schematically in **34**. If the downward perturbation is strong enough to shift 40 below 38, a distortion will be energetically favourable. Likewise, for the K' point we expect a situation such as **35**. If the two levels (38, 39) are perturbed strongly enough, a distortion is preferred for that k point. The actual situation, as represented by our band calculations is shown in figure 19. Here we have chosen a distortion parameter, ε, which interpolates linearly between the undistorted octahedral $ReSe_2$ structure and the experimentally observed one.

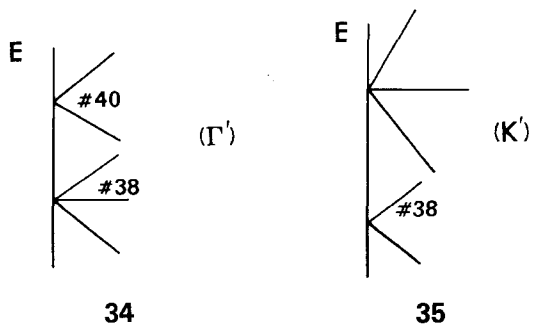

Figure 19 is a Walsh diagram for two points, the most important ones, in the BZ. Similar things happen at both. Due to the lowered symmetry several avoided crossings occur. The most important higher two orbitals (37 and 38) are pushed down by the presence of orbital 40, which is moved to lower energy by the geometrical perturbation at the Γ point, and 39 at the K point. As a result, early on (say at around $\varepsilon = 25\%$

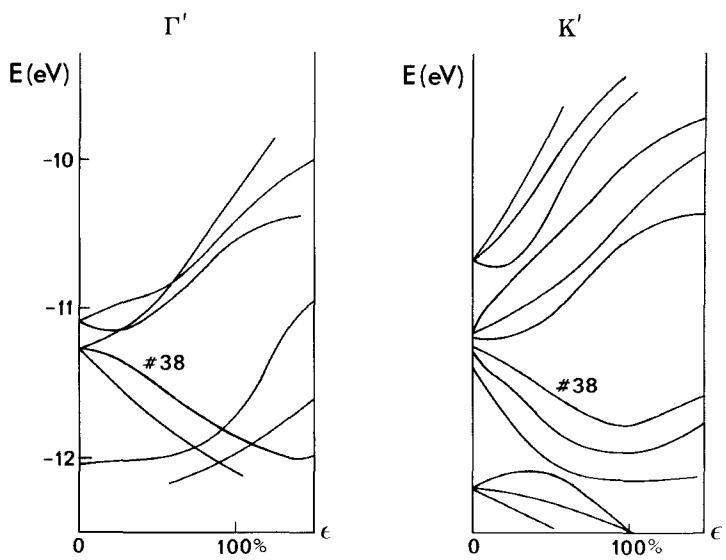

Figure 19. Walsh diagram for the distortion of $ReSe_2$ for two points in the BZ as metal–metal bonding develops. The distortion coordinate, ε, connects the ideal undistorted ($\varepsilon = 0$) and the distorted experimental ($\varepsilon = 100\%$) structures linearly (Kertesz and Hoffmann 1984 a).

distortion) the highest occupied levels move sharply to lower energy, driving the lattice to distort. How strong is this electronic distortion force? It is actually felt throughout the whole BZ, although to a varying degree. According to our calculations, the energy gain per Re_4Se_8 units ($\varepsilon = 100\%$) is $-2{\cdot}54$ eV at Γ', $-4{\cdot}55$ eV at K' and $-3{\cdot}45$ eV on the average over the whole BZ.

We can also look at the calculated total energy difference between the experimentally observed ($ReSe_2$) and the undistorted structure as a function of electron count. This is done in table 2.

Table 2. $\Delta E = E(\varepsilon = 0) - E(\varepsilon = 100\%)$ for Re_4Se_8, in electron volts, as a function of d electron count.

d^n	d^0	d^1	d^2	d^3	d^4	d^5
ΔE	$-0{\cdot}97$	$0{\cdot}26$	$1{\cdot}15$	$3{\cdot}45$	$1{\cdot}10$	$-8{\cdot}84$

The particularly large energy gain at the d^3 (Re) electron count coincides with the fact that the particular distortion observed in $ReSe_2$ is energetically favourable.

One consequence of this distortion is the opening of an energy gap in the band structure. The magnitude of the calculated indirect gap (0·89 eV) lies close to the experimental (optical) gap (Wildervanck and Jellinek 1971) of 1·15 eV for $ReSe_2$ and 1·33 eV for ReS_2, respectively. The calculated direct gap at Γ is 1·16 eV.

The above discussion of the distortion of $ReSe_2$ allowed us to trace back the driving force for the distortion to a Jahn-Teller-type splitting of orbitals. The splitting at small distortion values does *not* occur *at the Fermi level*, although close to it, but the level splitting is large enough to move the Fermi level, whose exact position is not essential for the actual distortion to occur.

This is in contrast to other, quite familiar, distortions widely occurring in quasi-one- and two-dimensional systems, as e.g. polyacetylene, or several d^1 transition-metal dichalcogenides, which are known under the names of Peierls distortion and periodic lattice distortions coupled to charge-density waves (Friend and Jerome 1979). For these instabilities, the periodicity of the distortion is related to particular dimensions and forms of the Fermi surface, which is often not commensurate with the periodicity of the lattice. These instabilities are most easily visualized in the language of energy band theory; the existence of large parallel 'nesting' regions of the Fermi surface separated by a single wave-vector $2k_F$ leads to a strong scattering of the electrons with momentum $\pm k_F$, splitting their energy strongly. Thus, an energy gap opens up and the system is stabilized. The periodicity of the potential, and thus that of the periodic lattice distortion, is tied in this picture to the particular k_F. Without going further into this complex subject, it is already clear that the case of $ReSe_2$ is different, in that neither the shape of the Fermi surface nor its energy is determining the particular 'clustering' distortion of this semiconductor.

What then determines this deformation? Since three electrons occupy the three-d-type bands, the distortion is such as to open a gap in the middle of it. Thus, the ratio of the number of bonding and antibonding regions should be roughly 1 : 1. For this to occur, doubling of the unit cell may be sufficient. However, for a system with the unit cell of Re_2Se_2 the number of short and long contacts cannot be 1 : 1 (in a lattice derived from a hexagonal one), in contrast to a one-dimensional system where this is easily fulfilled (see, e.g. the case of polyacetylene). On the other hand, for four units, this

condition may be fulfilled with the formation of the diamond-shaped clusters of the experimental $ReSe_2$ structure.

In any molecular or extended system the overlap populations signal the way for a molecular distortion. By way of example let us step back from the crystal case to a molecular one, the simple Jahn-Teller system of cyclobutadiene (**36**). When $r_{12}=r_{23}$ the

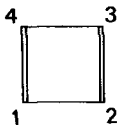

36

ground state is degenerate in Hückel theory. The overlap populations p_{12} and p_{23} are undetermined, they depend on the arbitrary choice of the occupied subspace within the two degenerate molecular orbitals (MOs). However, the slightest distortion towards a geometry with $r_{12}-r_{23}\neq 0$ leads to π overlap population $p^{\pi}_{12}<0$ and $p^{\pi}_{23}>0$, which do not depend strongly on $r_{12}-r_{23}$, as illustrated by an MO calculation for C_4H_4 on figure 20. In a similar way, it is informative to look at the overlap populations for the different metal–metal bonds in $ReSe_2$ at the very beginning of the distortion. For technical reasons (numerical stability), we have chosen a 1% deformation. Table 3 summarizes some of these overlap populations, at different electron counts.

The d^3 count is particularly suitable for the formation of the chains as indicated in **32**: all bonds which will become shorter have larger overlap populations, those which will become larger are close to zero at d^3. The difference does not change dramatically even at 3% deformation, in analogy to the cyclobutadine case. Thus, the wavefunction at very small deformation is already pointing into the direction of the actual deformation. The bond orders at the fully developed deformation are indicative of slight metal–metal bonding in the chains. We may conclude this section by answering the question posed in the subtitle; the distortion of $ReSe_2$ shows all the significant features of the molecular Jahn–Teller distortion.

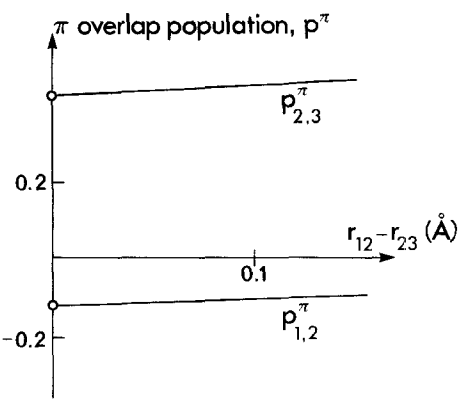

Figure 20. π-Overlap populations for cyclobutadiene as a function of $r_{12}-r_{23}$ ($r_{12}+r_{22}=$const). The empty circles at $r_{12}-r_{13}=0$ indicate that the values are undetermined in Hückel theory.

Table 3. p_{ij} overlap populations (× 1000) averaged over the whole BZ, as a function of electron count, and deformation for Re_4Se_8. Numbering according to **32**.

	$\varepsilon=1\%$					$\varepsilon=3\%$	$\varepsilon=100\%$
	d^0	d^1	d^2	d^3	d^4	d^3	d^3
Intrachain							
2,3	27	40	37	13	−18	21	193
1,3	26	37	36	10	−18	13	143
1,2	26	37	36	10	−18	12	140
1,4′	26	36	36	10	−19	11	89
Interchain							
4,1″	26	33	33	−0·4	−22	−1	−32
2,1″	26	34	34	2	−20	2	−37

6. The graphite to diamond transformation

In the last descriptive section we shall discuss an orbital model for a solid-state transformation, in particular the reaction starting from graphite and leading to diamond (Kertesz and Hoffmann 1984 b). Aside from its intrinsic interest, it will turn out that this transformation bears resemblance to certain possibly concerted chemical reactions which have symmetry-related constraints (Woodward and Hoffmann 1970). Burdett and Price (1982) have elegantly applied the ideas of orbital correlation diagrams to solid-state polymorphic transformations, and our analysis extends their work.

The basic geometries of the two allotropes, rhombohedral graphite and diamond, are well known. Three coordinates define the structures and the reaction coordinate: r, the CC distance within the layer ($r_G=1{\cdot}40$ Å, $r_D=1{\cdot}54$ Å); R, the CC distance between layers ($R_G=3{\cdot}35$ Å, $R_D=1{\cdot}54$ Å), the angle θ between the perpendicular to the layers direction (z axis) and a CC bond within a layer ($\theta_G=90°$, $\theta_D=109{\cdot}47°$).

All the coordinates change continuously during a hypothetical concerted transformation, but it is R which is most changed, and causes the large reduction in volume. Then choosing R as an independent variable, we have optimized the other two parameters, r and θ, along the reaction path, using extended Hückel band calculations. Rhombohedral symmetry was maintained along the reaction path.

The computed energy profile is indicated in figure 21. The extended Hückel method is not reliable for absolute energies, especially when bond distance changes are involved. In the case at hand the instability of diamond relative to graphite is much exaggerated. Nevertheless, we have substantial experience with extracting reliable orbital and symmetry arguments from the method, and it is in this sense that we will eventually use the computation.

Let us examine some features of the computed reaction path. The dashed line in figure 21 corresponds to the total energy with the graphite structure with $\theta=90°$ and $r=r_g$ fixed. For R close to R_G the two curves run close, thus the energy gain due to the relaxation of θ and r is not significant.

Nearing the transition state (TS), the other two coordinates become very much involved. The calculations give a transition state for this reaction in which the pyramidalization is almost complete, the in-plane bonds have almost reached their diamond values, only the interplane bonds are very long and different from those in diamond. The graphite π delocalization is completely lost.

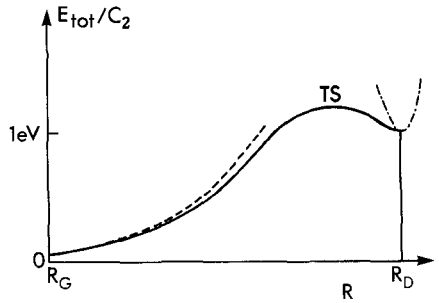

Figure 21. Total energy per two carbon atoms during the graphite to diamond transformation: (——) fully optimized, (– – –) rigid planes of graphite in a parallel approach, (–·–·) energy profile of the diamond structure. TS indicates the transition state (Kertesz and Hoffmann 1984 b).

The total energy is an average over the symmetric unit cell of the reciprocal space, the BZ. However, as in the case of molecules, the nodal structure of the wavefunction is preserved to a great extent, even in quasi-symmetrical cases. Thus, even off the high symmetry points or lines and planes of the BZ, but in their vicinity, the consequences of the symmetry are felt strongly. Therefore, these high symmetry points carry measurable weights in the averages over the BZ.

For the Γ point of diamond there is full *s-p* separation, due to the tetragonal symmetry. One of the triply degenerate sets ($2p_z$) has the orbital diagram depicted in **37**, together with the π and π^* orbitals in graphite. Also included are the related orbitals at *T*. The symmetry correlation in **37** is such that along the reaction coordinate the levels cross somewhere.

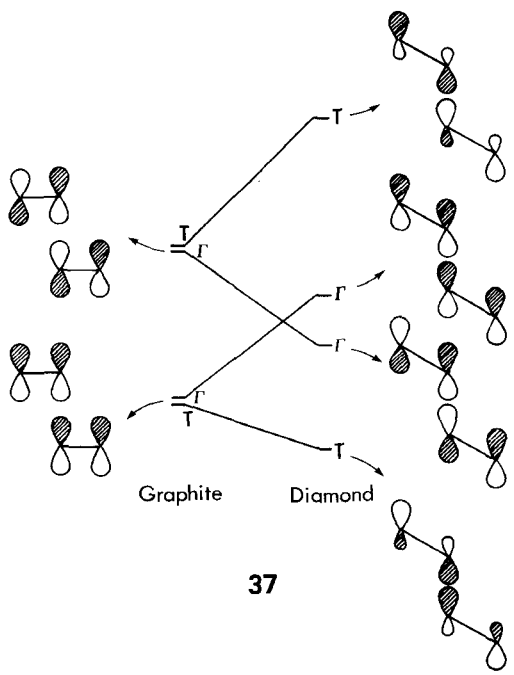

37

While there are many similarities between level correlations and curve crossing in discrete molecules and similar phenomena is extended structures, there are important differences to note. First, the two crossing levels on the correlation diagram **37** *do not* correspond to the highest occupied (HO), or lowest unoccupied (LU) levels. Those HO or LU levels are dependent on the band structure as a whole, and they are not even necessarily at the zone edges or high symmetry points. This leads to the second important difference: the transition state, as well as a range of states on both sides of the transition state, TS, corresponds to partly filled, thus *metallic* band, structures. This is illustrated in figure 22 through the changes of the densities of states as the reaction proceeds. If we were to draw Walsh-type diagrams for many k points in the BZ, we could see how the changes of the densities of states come about. But we do not think this is necessary here. Due to the very strong perturbations of the p states on **37** the Γ point of the band structure is moved so strongly, that the filling has to become partial, leading to a metallic band structure along the transition.

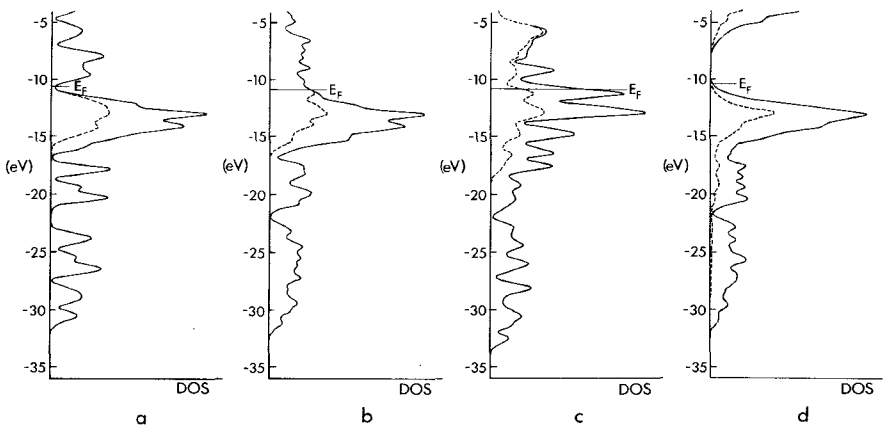

Figure 22. Valence electron (DOS) along the graphite to diamond transformation. (*a*) graphite; (*b*) compressed graphite, unbuckled planes at 2·67 Å distance; (*c*) the computed transition state, TS; (*d*) diamond. The dashed projections are for $2p_z$ orbitals. Note the large DOS at the Fermi energy, E_F, in cases (*b*) and (*c*) (Kertesz and Hoffmann 1984 b).

This discussion accounts for the reversible decrease of resistivity, followed by an irreversible increase in the same observable as the pressure is raised in graphite (Drickamer *et al.* 1966).

The above model explains the high stability of the metastable diamond phase: after high pressure has put the system over the (symmetry-related) barrier, it would require negative hydrostatic pressure to reverse the transition.

The fact that the TS structure is unstable, and that it is metallic, could possibly imply that its distortion to the insulating diamond, or to the semimetallic graphite is in some way related to a Peierls-like effect. This is not so, because the degeneracy in the Peierls case is related to symmetry, whereas here it is an accidental degeneracy originating from a level crossing.

The actual mechanism of the high-pressure transformation of graphite to diamond is certainly much more complex than the model we have studied. First, rhombohedral

graphite is rare, and is always found together with hexagonal graphite (Donohue 1974). Hexagonal graphite, however, cannot yield a diamond structure, unless the approach of the graphite planes is coupled to some in-plane slip of some of these planes. For instance, slipping leading to AA packing will lead to a hexagonal diamond. A more complicated slip pattern to ABC packing (effectively rhombohedral) can then lead to cubic diamond. A further complication is that catalysts and heat treatment change the kinetics of the transformation appreciably (Bundy *et al.* 1973). If shear is applied in addition to high pressure, the minimal temperature and pressure required for the transformation is lowered (Zhorin *et al.* 1982). This fits well into the present picture. The interconversion of graphite and diamond may also involve nucleation and growth. These could be thought of as solid-state analogues of non-concerted or step-wise processes, which we know intervene in the molecular case when orbital symmetry barriers are imposed.

7. Remarks on the one-electron theories

The general question, why the simple sum of one-electron energies may be of any use in estimating total energies has, of course, intrigued theoretical chemists (see, for example, Phillips and Van Vechten 1970, Skriver 1982, McWeeney 1979, Glimarc 1979, Mechrotra and Hoffmann 1978).

Perhaps the most direct justification is based on an observation of Politzer (1976) according to which

$$E_{\text{tot}} = \tfrac{3}{7}(V_{\text{ne}} + 2V_{\text{nn}}) + \Delta \tag{28}$$

where V_{ne} is the nuclear–electron attraction, V_{nn} is the nuclear–nuclear repulsion and Δ is a small correction. Then, using the virial theorem, one can obtain the following relationship

$$E_{\text{tot}} \cong K \sum \varepsilon_n(k) \tag{29}$$

where K is a constant. This gives a theoretical basis for putting $\Delta E = 0$ in the fundamental equation (15) (Ruedenberg 1977, Kertesz *et al.* 1978).

7.1. *The Hamiltonian*

The remarkable ability of one-electron effective Hamiltonians (H_{eff}) to describe energy bands and bonding in a wide variety of solids is well documented (Harrison 1980, Bullett 1980, Kelly 1980, Burdett 1984). In these schemes H_{eff} does not depend on the wavefunction $\psi_{nk}(r)$, which is usually expressed as a linear combination of atomic orbitals (1).

Approximations for H_{eff} within an AO basis, $\chi_i(r)$, are used for various purposes. The following are the most well-known models, all of which we consider as variants of the extended Hückel theory (EHT).

The Wolfsberg–Helmholz (1952) form is defined by

$$H_{ii} = -I_i \ (I_i\text{: ionization potential}) \quad . \tag{30a}$$

$$H_{ij} = -0{\cdot}5KS_{ij}(I_i + I_j), \qquad S_{ij} = \langle \chi_i(r)/\chi_j(r) \rangle \tag{30b}$$

Further form are the Cusachs–Reynolds (1965), the Ballhausen–Gray (1962), the Pantelides–Harrison bond-orbital approximation (1976), the weighted H_{ij} formula (Ammeter *et al.* 1978) and Bullett's scheme (1980) based on Anderson's chemical pseudopotential (CP) (Weeks *et al.* 1973). The latter has been rather successful in

describing the equilibrium bond distances. (It is well known that the one-electron method gives, in some instances, too short covalent bond distances.) The CP scheme involves a non-Hermitian matrix D_{ij}.

$$D_{ii}=\varepsilon_i \tag{31 a}$$

$$D_{ij}=\langle\phi_i|V_i'|\phi_j\rangle \qquad (i\neq j) \tag{31 b}$$

where ϕ_i are atomic Hartree–Fock orbitals, and V_i' is the difference of the full crystal Hamiltonian H from the isolated atom Hamiltonian. Note that $\langle i'|V_i|j\rangle \neq \langle i|V_j|j\rangle$. The matrix elements are evaluated by numerical integration,

$$D_{ij}=\int |r_m|<|r_n|\phi_i(r_m)\{V(r_m)-V(r_n)\}\phi_j(r_n)\,d^3r \tag{32}$$

where r_m and r_n are the position vectors r from each nucleus as coordinated system origins.

It can be shown that this formalism becomes equivalent to the Wolfsberg–Helmholz one under the conditions that

$$D_{ij}+D_{ji}=(K-1)S_{ij}(H_{ii}+H_{jj}) \tag{33}$$

Some further 'non-empirical' non-self-consistent schemes are being used by various research groups. For example, Bredas *et al.* (1982) have applied the Nicolas–Durand (1979) effective Hamiltonian techniques and arrived at reasonably good energy bands for conjugated polymers. Although based on sample *ab initio* calculations, this method is in fact very closely related to the above extended Hückel methods, as can be judged from both the final form of the theory and the numerical results it yields (e.g. the obtained gaps are somewhat too small). Unfortunately it is not clear whether this technique provides a reasonable core repulsion.

Woolley (1981) has studied the connections of CP and EHT, but his formal analysis does not give a clue as to why the CP formulation is more successful in predicting bond distances than EHT is. Probably it is not the formalism itself, as the Hamiltonian matrix of EHT is directly expressible in terms of the **D** matrix elements of the CP theory

$$\mathbf{H}=\mathbf{SD} \tag{34}$$

However, the way the integrals are calculated is different, and approximation (33) becomes less valid for short interatomic distances. This fact was realized earlier and other suggestions to overcome the high density difficulty involve, for instance, use of additional semiempirical atom–atom repulsion terms (Anderson and Hoffmann 1974).

Let us now turn to some of the merits and disadvantages of the one-electron theories.

7.2. *Advantages and disadvantages of one-electron theories for solids*

Perhaps the main formal advantage of the non-self-consistent theories is the applicability of a simple *perturbation theory* (PT) (Hoffmann 1971) which becomes invalid using more sophisticated Hamiltonians as, for instance, self-consistent field ones. The simplest form of this PT makes predictions about *substitutional preferences* which are quite important issues in chemistry. Examples of the type of logic involved can be found in standard textbooks on the Hückel theory (see, for example, Heilbronner and Bock 1976). The main point is that the change of the atomic Coulomb

integrals $\delta\alpha_i$ induces a change in the total energy. Up to first order (suppose the resonance integrals are unchanged):

$$\delta E = \sum_i q_i \delta\alpha_i \tag{35}$$

where q_i are the atomic π-charge densities calculated for an unperturbed homoatomic system. Then predictions can be made for substitional preferences because the largest stabilization occurs for a substitution of more (less) electronegative atoms with larger (smaller) q_i values. Of course, these predictions could be made by performing a full calculation (at the one-electron, or a more sophisticated, level) but the advantage we gain by doing PT is that we can make a theoretical connection between chemically related systems. By performing numerical calculations and subsequently picking the most stable one is also a prediction, but of another type: it is more like a numerical experiment which does not give conceptual relationships between the molecules or solids studied. There are not too many solid-state substitutional preference studies published yet, although a large number of solid-state structural problems are of this kind. Regarding a few remarkably successful predictions, we refer to a review of Burdett (1984).

The *rigid band*, or average band, *model*, discussed above in some detail, is useful for comparing the energetics of related solids with different electron counts. This is another area where the applicability of PT is crucial. The average band structure can be viewed as one corresponding to some hypothetical 'average' chemical elements, and the actual compounds are represented by parameters deviating not too much from these average ones. As long as deviations are small, these changes can be followed by PT again, with the benefit of making direct comparison and observations of trends regarding related but distinct compounds. The rigid band model is also applicable in situations where electron counts are changed due to varying charge transfer. Here neglect of self-consistency effects in the Hamiltonian makes it possible to use the wavefunction for one amount of charge transfer to predict the properties of the system for another amount of charge transfer.

The study of *Peierls*-type *distortions* is a further area where it may be beneficial to use simplified Hamiltonians. The knowledge of the nodal structure of the wavefunction at and around the Fermi level often contains information as to how the structure may be susceptible to lattice distortions and how these tendencies are related to specific electron counts (see, for example, Kafafi and Lowe 1984). Although self-consistent field (SCF) calculations showing instabilities towards different kinds of charge density waves, such as diagonal and off-diagonal charge density waves or spin density waves (Kertesz 1982, Whangbo 1983), may be used beneficially to study tendencies towards distortions in a given system, again studies based on simple non-SCF Hamiltonians have the advantage of allowing the investigator to make connections among related but distinct systems.

Recognition of natural building blocks or *fragments* is facilitated by the use of non-SCF Hamiltonians (see, for example, Hoffmann 1982 and references therein). A fragment molecular orbital (FMO) analysis for solids is also possible. This is a way to recognize the localized building blocks from which a solid is made up. Fragmentation, as any localized picture in quantum chemistry, is not unique. In some cases the interactions suggest a natural fragmentation: for instance, in solid hydrogen fluoride the localized orbitals are largely concentrated on the HF molecules (Kertesz *et al.* 1979). In other cases attempts to recognize localized bond orbitals from full band calculations

have been successful (Surjan *et al.* 1983). However, non-SCF Hamiltonians have the formal benefit that virtually any fragmentation is possible and thus fragmentation can be tailored according to the chemical building blocks and molecular analogies. An enlightening example for this kind can be found in a recent study of the Chevrel phases by Hughbanks and Hoffmann (1983). In this work a connection is made between the electronic structure of infinite $(Mo_3X_3^-)_\infty$ chains (X=S, Se, Te) and $Mo_{3n}X_{3n+2}$ clusters. In establishing these types of connections, which ought to be obvious from a chemical point of view, use is made of the molecular orbitals of common fragments (Mo_3 units in this case) to enable us to identify the common features of the Mo–X and Mo–Mo bonding in these systems.

As to the limitations of the non-SCF theories, their main drawback is that they are inferior in some of their quantitative predictive capabilities to *ab initio* or SCF semiempirical theories. There are several areas where *ab initio* theories are rather poor; the prediction of too large gaps by the exact exchange theories and the typical underestimation of it by local density theories is well known (Kertesz 1982, Sham and Schluter 1983, Perdew and Levy 1983). Well-described *unoccupied orbitals* are essential in some of the above-mentioned favourable features of the non-SCF theories. This is related to the fact that the energy gaps of these calculations tend to be so reasonable. The present author believes that more work is needed to clarify this point theoretically. Nevertheless, the recent successes of the density functional theories in predicting stable geometries and energy differences between closely related phases are remarkable (see, for example, Yin and Cohen 1982, Chelikowsky and Louie 1984). Even the dependency of the gap on high pressure seems to come out right (Chang *et al.* 1984). Although the simple theory can be used to map out the general features of the bands and energetics, more elaborate calculations are needed to account for details accurately. Especially problematic is the energetic comparison of related structures with different coordination numbers, such as that of α-Si (4 coordinated) and β-Si (6 coordinated) (see e.g. Biswas and Kertesz 1984). The successful applications of *topological* considerations comparing stabilities of different structures (Burdett 1984) are also probably limited by the same drawback of the simple theory (T. Hughbanks 1984, personal communication).

Simple (non-SCF) one-electron theories are usually at their weakest in applications to very polar systems. Nevertheless, as far as stability differences of related structures are concerned, Hückel type calculations may be useful guides, as demonstrated recently by the study of NbO and TiO by Burdett and Hughbanks (1984). This is again an area of application, where results are better than they 'ought to be', due to compensation of errors. We are convinced that the two approaches, the simple non-SCF kind and the sophisticated *ab initio* type, are supplementing each other very well and are contributing to our fundamental understanding of the electronic levels and orbitals in solids.

In this review we have attempted to present in an elementary way how much energy band calculations can do for solid-state chemical problems. We have sampled from a very large literature to pinpoint a few typical problems: distortion of regular metallic structures into insulating ones with lower symmetry, effects of charge transfer and comparison of stabilities of related solid-state structures.

Acknowledgments

I am indebted to Professor J. Thomas for encouraging me to write this account. I have benefited from the stimulating discussions with Professor R. Hoffmann and his

research group over an extended period of time. I also thank Dr. T. Hughbanks for his valuable comments on the manuscript. The research reported here has been supported by various generous grants: a KKA grant from the Hungarian Academy of Sciences, an NSF grant (DMR 7681083) through the Materials Science Center at Cornell University and a Cotrell Research Grant from the Research Corporation. Acknowledgment is also made to the donors of the Petroleum Research Fund, administered by ACS, for partial support of this work. I am indebted to Mrs. K. A. Bayne for the expert typing, and Mrs. A. Pope for the skilful drawings.

References

ALCOCK, N. W., and KJEKSHUS, A., 1965, *Acta chem. scand.*, **19,** 79.
AMMETER, J. H., BURGI, H. B., THIBEAULT, J. C., and HOFFMANN, R., 1978, *J. Am. chem. Soc.*, **100,** 3686.
ANDERSON, A. B., and HOFFMANN, R., 1974, *J. chem. Phys.*, **68,** 1744.
ANDERSON, P. W., 1968, *Phys. Rev. Lett.*, **21,** 13.
ANDERSON, P. W., 1969, *Phys. Rev.*, **181,** 25.
BALLHAUSEN, C. J., and GRAY, H. B., 1962, *Inorg. Chem.*, **1,** 11.
BARON, F., FLANDROIS, S., HAUW, C., and GAULTIER, J., 1982, *Solid St. Commun.*, **42,** 759.
BATRA, I. P., CIRACI, S., and RUDGE, W. E., 1977, *Phys. Rev.* B, **15,** 5858.
BISWAS, R., and KERTESZ, M., 1984, *Phys. Rev.* B, **29,** 1791.
BLOCH, F., 1928, *Z. Phys.*, **52,** 555.
BLUMEN, A., and MERKEL, CH., 1977, *Phys. Stat. Sol.* (b), **83,** 425.
BOON, M. R., 1971, *Theor. chim. Acta*, **23,** 109.
BOZOVIC, I. B., and DELHALLE, J., 1984, *Phys. Rev.* B, **29,** 4733.
BREDAS, J. L., CHANCE, R. R., BAUGHMAN, R. H., and SILBEY, R., 1982, *J. chem. Phys.*, **76,** 3673.
BULLETT, D. W., 1975, *Phil. Mag.* B, **32,** 1063.
BULLETT, D. W., 1980, *Solid St. Phys.*, **35,** 129.
BUNDY, F. R., STRONG, H. M., and WENTORF, R. H., JR., 1973, *Chem. Phys. Carbon*, **10,** 213.
BURDETT, J. K., 1984, *Prog. Solid State Chem.* (in the press).
BURDETT, J. K., and HUGHBANKS, T., 1984, *J. Am. chem. Soc.* (in the press).
BURDETT, J. K., and LEE, S., 1984 (to be published).
BURDETT, J. K., and PRICE, S. L., 1982, *Phys. Rev.* B, **25,** 5778.
CALLAWAY, J., 1964, *Energy Band Theory* (New York: Academic Press).
CHANG, K. J., FROYEN, S., and COHEN, M. L., 1984, *Solid St. Commun.*, **50,** 105.
CHELIKOWSKY, J. R., and LOUIE, S. G., 1984, *Phys. Rev.* B, **29,** 3470.
CHIANG, C. K., HEEGER, A. J., and MACDIARMID, A. G., 1979, *Ber. Bunsenges*, **83,** 407.
CHING, W. Y., HARRISON, J. G., and LIN, C. C., 1977, *Phys. Rev.* B, **15,** 5975.
COHEN, M. J., GARITO, A. F., HEEGER, A. J., MACDIARMID, A. G., MIKULSKI, C. M., SARAN, M. S., and KLEPPINGER, J., 1976, *J. Am. chem. Soc.*, **98,** 3844.
COULSON, C. A., and STREITWIESER, A., JR., 1965, *Dictionary of π-Electron Calculations* (San Francisco: W. H. Freeman).
CUSACHS, L. C., and REYNOLDS, J. W., 1965, *J. chem. Phys.*, **43,** 5160.
DONOHUE, J., 1974, *The Structure of the Elements*, 2nd edn. (Malabar, Florida: Krieger).
DRICKAMER, H. G., LYNCH, R. W., CLENDENEN, R. L., and PEREZ-ALBUERNE, E. A., 1966, *Solid St. Phys.*, **19,** 135.
FAUSTER, TH., HIMPSEL, F. J., FISHER, J. E., and PLUMER, E. W., 1983, *Phys. Rev. Lett.*, **51,** 430.
FINCHER, C. R., JR., PEEBLES, D. L., HEEGER, A. J., DRUY, M. A., MATSUMURA, Y., MACDIARMID, A. G., SHIRAKAWA, H., and IKEDA, J., 1978, *Solid St. Commun.*, **27,** 489.
FINCHER, C. R., JR., CHEN, C. E., HEEGER, A. J., MACDIARMID, A. G., and HASTINGS, J. B., 1982, *Phys. Rev. Lett.*, **48,** 100.
FISHER, J. E., 1980, *Physica* B, **99,** 383.
FRIEND, R. H., and JEROME, D., 1979, *J. Phys.* C, **12,** 1441.
FRIESEN, W. I., BERLINSKY, A. J., BERGERSEN, B., WEILER, L., and RICE, T. M., 1975, *J. Phys.* C, **8,** 3549.
GLIMARC, B. M., 1979, *Molecular Structure and Bonding* (New York: Academic Press).
HARRISON, W. A., 1980, *Electronic Structure and Properties of Solids* (San Francisco: W. H. Freeman).
HEINE, V., 1960, *Group Theory in Quantum Mechanics* (Oxford: Pergamon Press).
HEILBRONNER, E., and BOCK, H., 1976, *The HMO Method and Its Applications*, Vol. 1 (New York: Wiley).

HEROLD, H., 1981, *Intercalation Compounds*, edited by L. Pietronero and E. Tosatti (Berlin: Springer-Verlag), p. 7.
HOFFMANN, R., 1963, *J. chem. Phys.*, **39,** 1397.
HOFFMANN, R., 1971, *Accts Chem. Res.*, **4,** 1.
HOFFMANN, R., 1982, *Angew. Chem.* (int. ed.), **21,** 711 (G.E. 725).
HOLZWARTH, N. A. W., 1983, *Intercalated Graphite*, (edited by M. S. Dresselhaus, G. Dresselhaus, J. E. Fisher and M. J. Moran (Amsterdam: North-Holland).
HÜCKEL, E., 1931, *Z. Phys.*, **70,** 204.
HUGHBANKS, T., and HOFFMANN, R., 1983, *J. Am. chem. Soc.*, **105,** 3528.
HUGHBANKS, T., HOFFMANN, R., WHANGBO, M. H., STEWART, K. R., EISENSTEIN, O., and CANADELL, E., 1982, *J. Am. chem. Soc.*, **104,** 3976.
HULLIGER, F., 1976, *Structural Chemistry of Layer-type Phases*, Vol. 5, edited by F. Lévy (Boston: D. Reidel).
KAFAFI, S. A., and LOWE, J. P., 1984, *J. Am. chem. Soc.*, **106,** 5837.
KELLY, M. J., 1980, *Solid St. Phys.*, **35,** 296.
KERTESZ, M., 1982, *Adv. quant. Chem.*, **15,** 161.
KERTESZ, M., 1985, *Mol. Cryst. liq. Cryst.* (to be published).
KERTESZ, M., and HOFFMANN, R., 1983, *Solid St. Commun.*, **47,** 97.
KERTESZ, M., and HOFFMANN, R., 1984 a, *J. Am. chem. Soc.*, **106,** 3453.
KERTESZ, M., and HOFFMANN, R., 1984 b, *J. Solid St. Chem.*, **54,** 313.
KERTESZ, M., KOLLER, J., and AZMAN, A., 1978, *J. chem. Phys.*, **69,** 2937.
KERTESZ, M., KOLLER, J., and AZMAN, A., 1979, *Solid St. Commun.*, **30,** 329.
KERTESZ, M., and VONDERVISZT, F., 1982, *J. Am. chem. Soc.*, **104,** 5889.
KERTESZ, M., VONDERVISZT, F., and HOFFMANN, R., 1983, *Intercalated Graphite*, (edited by M. S. Dresselhaus, G. Dresselhaus, J. E. Fisher, and M. J. Moran (Amsterdam, North-Holland), p. 141.
KERTESZ, M., VONDERVISZT, F., and PEKKER, S., 1981, *Chem. Phys. Lett.*, **90,** 630.
KIVELSON, S., and CHAPMAN, O. L., 1983, *Phys. Rev., B*, **28,** 7236.
MATTHEISS, C. F., 1973, *Phys. Rev.* B, **8,** 3719.
LANDO, J. B., and THAKUR, M. K., 1984, *Synthet. Met.*, **9,** 317.
MCWEENEY, R., 1979, *Coulson's Valence* (Oxford: Oxford University Press).
MECHROTRA, P. K., and HOFFMANN, R., 1978, *Theor. chim. Acta*, **48,** 301.
NICOLAS, G., and DURAND, PH., 1979, *J. chem. Phys.*, **70,** 2020.
PANTELIDES, S. T., and HARRISON, W. A., 1976, *Phys. Rev.* B, **13,** 2667.
PEIERLS, R., 1955, *Quantum Theory of Solids* (Oxford: University Press).
PERDEW, J. P., and LEVY, M., 1983, *Phys. Rev. Lett.*, **51,** 1884.
PETTIFOR, D. G., 1977, *Calphad*, **1,** 305.
PHILLIPS, J. C., and VANVECHTEN, J. A., 1970, *Phys. Rev.* B, **2,** 2147.
PIETRONERO, L., and STRASSLER, S., 1981, *Phys. Rev. Lett.*, **47,** 593.
POLITZER, P., 1976, *J. chem. Phys.*, **64,** 4239.
RUEDENBERG, K., 1977, *J. chem. Phys.*, **66,** 375.
SALEM, L., 1963, *Molecular Orbital Theory of Conjugated Systems* (London: W. A. Benjamin).
SHAM, L. J., and SCHLUTER, M., 1983, *Phys. Rev. Lett.*, **51,** 1888.
SKRIVER, H. L., 1982, *Phys. Rev. Lett*, **49,** 1768.
STREET, G. B., and CLARKE, T. C., 1980, *Adv. Chem. Ser.*, **186,** 177.
WALLACE, P. R., 1947, *Phys. Rev.*, **71,** 622.
WEEKS, J. D., ANDERSON, P. W., and DAVIDSON, A. G. H., 1973, *J. chem. Phys.*, **58,** 1388.
WERTHEIM, G. K., VAN ATTEKREM, P. J. TH. M., and BASU, S., 1980, *Solid St. Commun.*, **33,** 1127.
WHANGBO, M.-H., 1983, *Accts Chem. Res.*, **16,** 95.
WHANGBO, M.-H., HOFFMANN, R., and WOODWARD, R. B., 1979, *Proc. R. Soc.* A, **366,** 23.
WILDERVANCK, J. C., and JELLINEK, F., 1971, *J. less-common Metals*, **24,** 73.
WILSON, J. A., and YOFFE, A. D., 1969, *Adv. Phys.*, **18,** 193.
WOLFSBERG, M., and HELMHOLZ, L., 1952, *J. chem. Phys.*, **20,** 837.
WOODWARD, R. B., and HOFFMANN, R., 1970, *The Conservation of Orbital Symmetry* (Weinheim: Verlag-Chemie).
WOOLLEY, R. G., 1981, *Nouv. J. Chim.*, **5,** 441.
YAMABE, T., TONAKA, K., OHZEKI, K., and YATA, S., 1982, *Solid St. Commun.*, **44,** 823.
YIN, M. T., and COHEN, M. L., 1982, *Phys. Rev.* B, **26,** 5668.
ZHORIN, V. A., KUSHNEREV, M. YA., SHASHKIN, D. P., NAGORNII, V. O., and ENIKOLONYAN, N. S., 1982, *Zh. Fiz. Khim.*, **54,** 2486.